



Breakdown of the electron-spin motion upon reflection at metal-organic or metal-carbon interfaces

F. Djeghloul, P. Dey,^{*} A. Hallal, E. Urbain, S. Mahiddine, M. Gruber, D. Spor, M. Alouani, H. Bulou, F. Scheurer, and W. Weber[†]

Institut de Physique et Chimie des Matériaux de Strasbourg, UMR 7504, CNRS-UdS, 23 rue du Loess, B.P. 43, 67034 Strasbourg Cedex 2, France

(Received 28 January 2014; published 14 April 2014)

Spin-polarized electron scattering experiments on different metal-organic and metal-carbon interfaces are performed. A completely unexpected behavior of the spin-motion angles as well as of related quantities as a function of the organic layer or carbon coverage is observed. In fact, by deposition of organic molecules or carbon onto ferromagnetic as well as nonmagnetic metal surfaces in the submonolayer thickness range, the electron reflection amplitude, i.e., both the reflectivity and the reflection phase, become spin independent. Our findings show that this behavior is a very general phenomenon which is independent of the electron energy and the choice of the metal as well as of the organic molecules and thus does not depend on the choice of the specific interface.

DOI: [10.1103/PhysRevB.89.134411](https://doi.org/10.1103/PhysRevB.89.134411)

PACS number(s): 75.70.Cn, 75.70.Rf, 72.25.Mk

I. INTRODUCTION

The study of the spin properties of metal-organic interfaces has recently received considerable attention [1–4] because of the prospect of developing a new generation of spin devices. In fact, organic spintronics, compared to its inorganic counterpart, offers many advantages. From the application standpoint, organic materials open the way to cheap, low-weight, mechanically flexible, chemically interactive, and bottom-up fabricated electronics. Furthermore, more efficient and innovative devices may be produced due to the long spin coherence time and spin-flip length, thanks to the weak spin-orbit coupling for light elements such as hydrogen, carbon, and nitrogen. Model vertical magnetoresistive devices have been produced using ferromagnetic metals or half-metals (see, e.g., Ref. [5]) as ferromagnetic electrodes and evaporated molecules such as phthalocyanine as tunnel barriers. Typically a few tens of percent of tunnel magnetoresistance has been obtained at low temperatures and a few percent at room temperature. These results show an interesting efficiency of spin transfer through organic materials.

From the fundamental point of view a lot of interesting physics takes place at the interface between ferromagnets and molecules [6,7]. Effects ranging from ferromagnetic coupling between a molecule's transition metal site and the ferromagnet [4] to metallic [8] spin-polarized states induced on the molecule by the interface's chemical bonds [9] have been subsumed in a recent analysis by Sanvito *et al.* [10] as signatures of a so-called spinterface that can craft spin-polarized transport [9,11]. In a very recent study some of us show that the spinterface created by the deposition of manganese phthalocyanine (MnPc) onto a ferromagnetic Co(001) film at room temperature is almost 100% spin polarized in the vicinity of the Fermi level [12].

Despite these promising features, a more complete understanding of the interfacial properties, in particular, the spin

transport through the molecular layer, requires the knowledge of how incident spin-polarized electrons are influenced when interacting with the molecular layer. The physics of this interaction is exactly the goal of the present study. By performing spin-polarized electron scattering experiments on different interfaces we observe a completely unexpected behavior of the spin-polarized reflection properties of these interfaces. In fact, by deposition of organic molecules or carbon in the submonolayer thickness range onto ferromagnetic or nonmagnetic surfaces, the electron reflection amplitude, i.e., both the reflectivity and the reflection phase, becomes spin independent. It is shown that this behavior is a general phenomenon which appears for all investigated electron energies and is independent of the choice of metal or organic molecules and, thus, does not depend on the choice of the specific interface. Despite this extensive study, we have no physical explanation for this intriguing behavior at the moment.

II. ELECTRON-SPIN MOTION

In the following the spin-polarization vector \mathbf{P}_0 of the incident electrons is perpendicularly oriented with respect to the magnetization \mathbf{M} of the ferromagnetic film. For simplicity, we consider in this section a completely polarized electron beam, i.e., $P_0 = 1$.

In the particular spin configuration which we consider here, the spin is a coherent superposition of a majority-spin and a minority-spin state. If \mathbf{P}_0 is along the x axis and \mathbf{M} along the z axis, these two spin states are represented by a (1,0) and a (0,1) spinor, respectively, and the initial spin configuration reads

$$\chi_0 \sim \begin{pmatrix} 1 \\ 0 \end{pmatrix} + \begin{pmatrix} 0 \\ 1 \end{pmatrix}.$$

The two partial waves have an arbitrary but identical phase prior to reflection at the surface of the ferromagnetic material. However, since the reflection process depends on the spin, the amplitudes of the two spin wave functions are different after

^{*}Present address: Department of Physics, National Institute of Technology Agartala, Jirania, Tripura 799046, India.

[†]wolfgang.weber@ipcms.u-strasbg.fr

reflection, and the total spin wave function will be

$$\chi \sim |r^\uparrow| e^{i\theta^\uparrow} \begin{pmatrix} 1 \\ 0 \end{pmatrix} + |r^\downarrow| e^{i\theta^\downarrow} \begin{pmatrix} 0 \\ 1 \end{pmatrix},$$

with $|r^{\uparrow,(\downarrow)}|$ the moduli of the spin-dependent reflection amplitudes and $\theta^{\uparrow,(\downarrow)}$ the corresponding reflection phases.

The expectation values of the Pauli matrices,

$$\sigma_x = \begin{pmatrix} 0 & 1 \\ 1 & 0 \end{pmatrix}, \quad \sigma_y = \begin{pmatrix} 0 & -i \\ i & 0 \end{pmatrix}, \quad \sigma_z = \begin{pmatrix} 1 & 0 \\ 0 & -1 \end{pmatrix},$$

yield the spin polarization vector \mathbf{P} of the electron beam after reflection:

$$\mathbf{P} = \frac{\langle \chi | \boldsymbol{\sigma} | \chi \rangle}{\langle \chi | \chi \rangle} = \begin{pmatrix} |r^\uparrow| |r^\downarrow| \cos(\theta^\downarrow - \theta^\uparrow) \\ |r^\uparrow| |r^\downarrow| \sin(\theta^\downarrow - \theta^\uparrow) \\ (|r^\uparrow|^2 - |r^\downarrow|^2)(|r^\uparrow|^2 + |r^\downarrow|^2)^{-1} \end{pmatrix}.$$

By introducing the intensity asymmetry

$$A = \frac{|r^\uparrow|^2 - |r^\downarrow|^2}{|r^\uparrow|^2 + |r^\downarrow|^2}$$

and the angle

$$\varepsilon = \theta^\downarrow - \theta^\uparrow,$$

the spin polarization vector becomes

$$\mathbf{P} = \begin{pmatrix} \sqrt{1 - A^2} \cos \varepsilon \\ \sqrt{1 - A^2} \sin \varepsilon \\ A \end{pmatrix}.$$

This corresponds to a precession of the polarization vector around the magnetization direction by an angle ε and a rotation by an angle ϕ in the plane spanned by \mathbf{P} and \mathbf{M} (see Fig. 1):

$$\phi = \arctan \left(\frac{A}{\sqrt{1 - A^2}} \right).$$

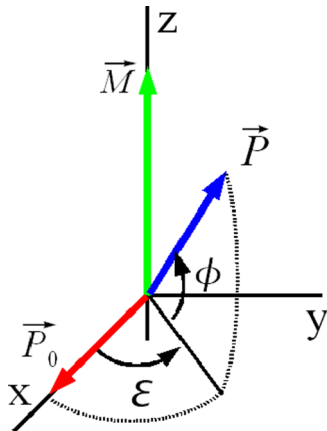


FIG. 1. (Color online) Illustration of the two types of motion of the spin-polarization vector. The initial spin polarization \mathbf{P}_0 precesses around the magnetization \mathbf{M} by an angle ε and rotates in the plane \mathbf{P} - \mathbf{M} by an angle ϕ .

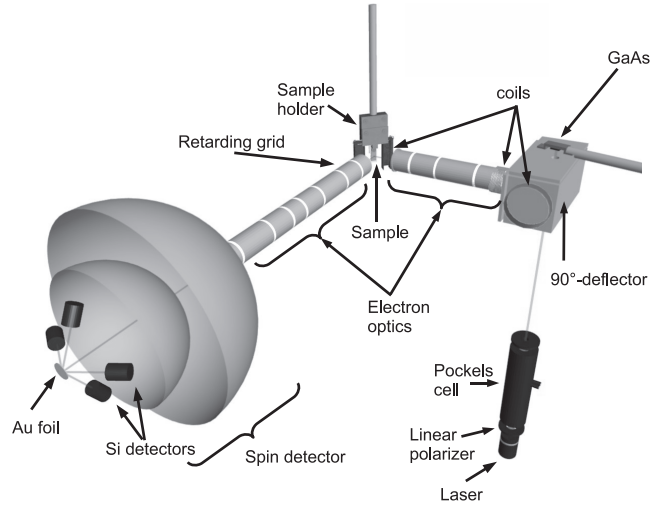


FIG. 2. The experimental setup consists of a laser diode that has a wavelength of 785 nm, a linear polarizer, a Pockels cell to create circularly polarized light and to change its helicity, an electrostatic 90° deflector, coils to rotate the direction of the initial spin polarization, a GaAs crystal, two transfer electron optics, a sample, coils to remanently magnetize the sample, a retarding field grid as energy analyzer, and four Si detectors and a Au foil for spin detection.

III. EXPERIMENT

A. Experimental setup

In order to investigate the spin motion of electrons upon reflection from a ferromagnetic surface, a spin-polarized electron scattering experiment is necessary, in which both the incident electrons are spin polarized and the spin state of the electrons after reflection is analyzed. The experiment is shown schematically in Fig. 2. A spin-polarized electron source based on a GaAs photocathode produces a transversely spin-polarized free electron beam of 25% spin polarization \mathbf{P}_0 [13]. By switching from right- to left-circularly polarized light for photoexcitation of spin-polarized electrons, the direction of the initial spin polarization can be inverted. By applying a combination of electric and magnetic fields to the electron beam, \mathbf{P}_0 can be rotated in any desired space direction. An unpolarized electron beam can also be produced by applying linearly polarized light. The electron beam impinges onto the sample at an angle of 45° with respect to the surface normal. The specularly reflected electrons are energy analyzed by a retarding grid analyzer that has an energy resolution of 0.3-eV FWHM. Besides the elastic electrons, there is a broad distribution of inelastically scattered electrons as well, which could be suppressed by applying a retarding field. Subsequently, the elastic electrons are accelerated to an energy of 100 keV to measure the transverse components of the spin-polarization vector via a Mott detector, which exploits the left-right asymmetry of electron scattering due to spin-orbit interaction [14]. The effective Sherman factor of the Mott detector is 0.2. To remove any experimental asymmetry (for instance, due to a misalignment of the electron beam with respect to the Mott detector), the direction in space as well as the relative alignment of \mathbf{P}_0 and \mathbf{M} must be interchanged, corresponding to four measurements. On reversing \mathbf{P}_0 , only

the precession angle changes sign, while on reversing \mathbf{M} , both the precession and the rotation angle change sign.

B. Samples

In the first step of the sample preparation different ferromagnetic films (Co and Fe) were deposited on different single-crystalline substrates (Cu(001), Ag(001), and Pt(001)) at room temperature from a rod heated by electron beam bombardment. Prior to deposition, the single-crystalline substrate was cleaned by several cycles of Ar-ion sputtering and annealing at 800 K. The film systems Co/Cu(001) and Fe/Ag(001) have been extensively investigated in the past [see, for instance, Refs. [15]–[18] for Co/Cu(001) and Refs. [19]–[23] for Fe/Ag(001)]. For the film system Fe/Pt(001), on the other hand, there have been few studies [24].

While Co films on Cu(001) are magnetized in-plane for all thicknesses, Fe films on Ag(001) and on Pt(001) exhibit a reorientation transition of the magnetization from out-of-plane to in-plane for thicknesses of 4 monolayers (ML) [25] and 2.2 ML [24], respectively. In all cases films of 15-ML thickness are deposited such that the magnetization of all ferromagnetic films lies in-plane.

In the second step of the sample preparation we deposit different organic molecules or amorphous carbon (a-C) onto the ferromagnetic film at room temperature. The organic molecules are evaporated by radiative heating, while carbon films are evaporated by electron beam bombardment and the evaporation rate is controlled by a quartz microbalance. In the electron scattering experiments the molecular or carbon films are grown as follows: at a typical growth rate of 1 ML/10 min, we make a deposition during times ranging from 15 s to several minutes. This is followed by a measurement that takes several minutes. Then the procedure is repeated. As a result, the effective deposition rate is usually much slower than 1 ML/10 min. The molecules studied are (see Fig. 3) unsubstituted phthalocyanine (H_2Pc ; $\text{C}_{32}\text{H}_{16}\text{N}_8\text{H}_2$), metal-substituted Pcs (CoPc, FePc, MnPc), 3,4,9,10-perylene tetracarboxylic dianhydride (PTCDA; $\text{C}_{24}\text{H}_8\text{O}_6$), coronene ($\text{C}_{24}\text{H}_{12}$), the alkane pentacontane ($\text{C}_{50}\text{H}_{102}$), and C_{60} . For the purpose of comparison we also evaporated a-C.

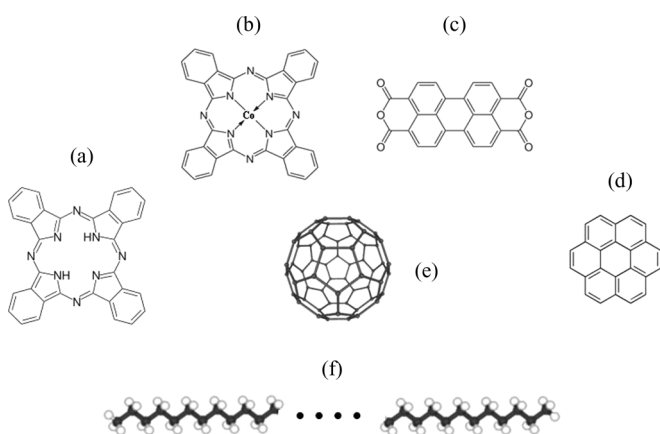


FIG. 3. Molecule of (a) H_2Pc , (b) metal-substituted Pc (here CoPc), (c) PTCDA, (d) coronene, (e) C_{60} , and (f) pentacontane.

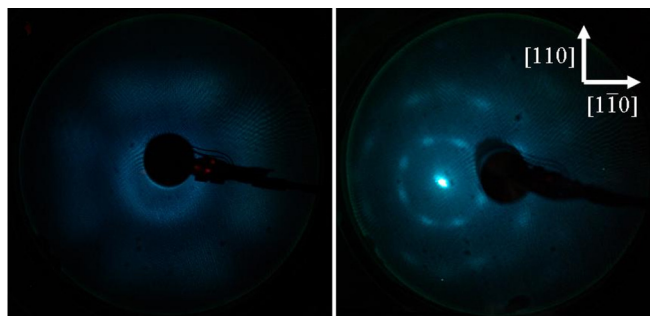


FIG. 4. (Color online) Left: LEED image of 0.6 ML CoPc on Cu(001) taken at 14.5 eV. Right: LEED image of 2 ML CoPc on Cu(001) taken in an off-center position such that the (0,0) beam appears to the left. The electron energy is 16.5 eV. Crystallographic axes of the Cu(001) crystal are indicated.

In certain cases where we have chosen Co(001) as the ferromagnetic film we deposited an intermediate layer of Au on top of the Co film in order to separate the molecules from the latter. In this way we were able to distinguish effects which are induced by a direct contact of the molecules with the ferromagnetic surface from those which are not induced by a direct contact. For characterization of the growth and structure of Au(111) films on top of Co(001) we refer the reader to our work on electron-spin motion in Au films on Co(001) [26]. The advantage of Au for the present study is the fact that at low electron energies it exhibits a very large inelastic mean free path (IMFP) [26]. This enables us to observe still a significant spin-motion signal from the Au/Co interface even for Au thicknesses as large as 15 ML.

In the following, two crucial questions are addressed: (i) Are we really depositing intact molecules? and (ii) How do we determine the thickness of the organic layers?

The first question has been addressed by studying exemplarily the system CoPc/Cu(001) by low-energy electron diffraction (LEED). These experiments at low coverages [see Fig. 4 (left) for 0.6 ML CoPc on Cu(001)] already show evidence of some ordering of the molecules on Cu(001) at room temperature, with a typical liquid-like first-order ring around the substrate (0,0) LEED spot and a fourfold-shaped second-order structure. This indicates strong nearest-neighbor ordering of the molecules but only weak long-range order.

For thicker CoPc films, 2 ML, the long-range ordering of the molecules on the Cu(001) surface becomes clear (see Fig. 4, right). Both first- and second-order spots are visible (third-order spots can be vaguely perceived), which indicates a very good long-range ordering. Very similar LEED images have been observed for CuPc on Cu(001) by Buchholz *et al.* [27]. The central message is therefore that we are indeed dealing with intact Pc molecules on the surface, as any disintegration of the Pc molecules would lead to a completely different LEED image. We note that in the case of MnPc molecules deposited onto Co(001) we also performed STM measurements which show undoubtedly intact molecules. Moreover, the Pc molecules are immune to damage by the incident electron beam, as the LEED image was stable for periods of hours under the LEED electron beam, not only at low energies but also at much higher energies (150 eV). Thus,

we can exclude any damage by our spin-polarized electron beam, as, first, the electron energies are usually much lower than the typical LEED energies, and second, the beam current in the spin-motion experiments is in the nanoampere range, while that of a LEED experiment is typically in the microampere range.

What is the thickness of the organic layers? To calibrate the organic layer thickness we exploit the fact that in most measurements reflectivity maxima appear that turn out to be at a thickness of 1 ML. In fact, the presence of islands for a noninteger coverage leads to a disordered surface such that diffuse electron scattering is enhanced. Consequently, the intensity of the specular elastic peak is reduced and becomes maximum only for a completed ML, for which the number of islands is minimum.

We note that intensity maxima can also be due to a quantum-well effect. In this case they can appear at any thickness, depending on the electronic band structure of the overlayer material. A quantum-well origin of at least most of the maxima observed in our experiments with the organic layers can, however, be excluded. In most experiments the reflectivity maxima for a given system appear always at the same deposition time (keeping the evaporation rate constant) independently of the primary electron energy. However, the thickness position of quantum-well-induced reflectivity maxima vary, in general, very strongly with the electron energy [26,28].

Combined measurements of the electron reflectivity and the Auger signal as a function of the organic layer deposition time allowed us to calibrate the thickness independently. For the particular case of CoPc on Co(001) a calibration using the reflectivity maximum, which is supposed to be at 1-ML coverage (interlayer distance is about 0.35 nm), results in IMFP values of 1.5 ± 0.15 and 3.3 ± 0.4 nm for electrons with kinetic energies of 277 eV (carbon Auger peak) and 782 eV (high-energetic Co Auger peak), respectively. These IMFP values are close to those given in the literature for many planar organic molecules. We refer here, for instance, to the theoretical work by Tanuma *et al.* [29] and the experimental work by Laibinis *et al.* [30], in which measurements of the IMFP have been performed in self-assembled MLs of *n*-alkanethiols on different metallic substrates. Both theory and experiment give quite similar values compared to those obtained in our experiments, namely, 1.5 and 2.7 nm for electrons of 277- and 782-eV kinetic energy, respectively. Similar Auger experiments with the other planar molecules (PTCDA, coronene, pentacontane) studied in the present work give similar values. We emphasize that combined Auger and STM measurements in the case of MnPc on Co(001), in which the MnPc coverage could be determined precisely, are consistent with the above results. This proves that our calibration method based on the reflectivity maxima, which appear in most cases at 1-ML coverage (in certain cases an additional maximum at 0.5 ML is identified), is correct. We note that all studied planar molecules have similar interlayer distances of about 0.35 nm.

Another independent check of the coverage is made in the case of CoPc/Co(001) and MnPc/Cu(001) by measuring the work function change of the substrate as a function of the organic layer coverage (see Sec. IV D). As the main changes

in the interface dipole usually appear during the deposition of the first ML, we expect a saturation for larger coverages. Indeed, the calibration of the organic layer thickness based on the reflectivity maxima is consistent with this fact.

In the case of C₆₀ layers we tried another way to independently calibrate the thickness. While the first layer of C₆₀ is chemisorbed on metallic surfaces [31–33] and therefore relatively strongly bonded, further layers are only weakly bonded via the van der Waals interaction. Consequently the first C₆₀ layer has a sublimation temperature that is substantially higher than that of the C₆₀ molecules in subsequent layers (450 K) [34]. In order to obtain 1 ML of C₆₀ we performed the experiment in the following way: In the first step we evaporated a thick C₆₀ film at room temperature. In the second step we heated the system at 600 K. We note that much higher temperatures, above 760 K, are necessary to lead to the fragmentation of C₆₀ molecules into graphite [34]. During heating we observed the Auger signal and realized after 10 min a dramatic decrease in the ratio of the Auger signals of C and Co, indicating the sublimation of C₆₀ layers and therefore a reduction of the C₆₀ coverage. As heating for an additional 30 min did not change the Auger ratio further, we strongly believe that we had obtained a stable ML of C₆₀. Knowing the ratio of the Auger signals of 1 ML C₆₀ on Co(001) we were thus able to calibrate the thickness scale in spin-motion experiments. We note that the above thickness calibration is consistent with the calibration based on the reflectivity maxima.

The thickness of the carbon layers (interlayer distance of 0.34 nm) was calibrated in the same way as for organic molecules. As for organic molecules, reflectivity maxima appear in the spin-motion experiments. By combining measurements of the electron reflectivity and of the Auger signal we obtained IMFP values of 0.8 ± 0.1 and 2.5 ± 0.4 nm for electrons with kinetic energies of 277 and 782 eV, respectively. These values are close to those found in a combined theoretical and experimental work [35] for graphite, namely, 0.8 and 2 nm for electrons of 277- and 782-eV kinetic energy, respectively. Again, the calibration via the reflectivity maxima allows us to determine the thickness in spin-motion experiments. We note that deposition of thicker carbon films (a few MLs) leads to a-C as evidenced by Raman measurements in which both the G (graphite) and the D (disorder) peak have comparable intensities (see Fig. 5). The G peak is close to the position of the single Raman line found at 1575 cm^{-1} on single crystals of graphite. This Raman line is present in all graphitic samples. The D peak at 1350 cm^{-1} , on the other hand, can be attributed to the strong disorder of the carbon film. Similar Raman spectra for a-C films are found in the literature [36].

IV. RESULTS AND DISCUSSION

A. Spin-motion experiments with CoPc layers on Co(001)

In order to study the spin motion of the reflected electrons from organic films, we started by measuring both the spin-integrated electron reflectivity and the electron-spin motion angles ε and ϕ as a function of the CoPc film thickness.

Figure 6(a) shows the reflectivity as a function of CoPc thickness at a primary electron energy $E - E_F = 7$ eV. After a sharp decay in the intensity it increases again and exhibits

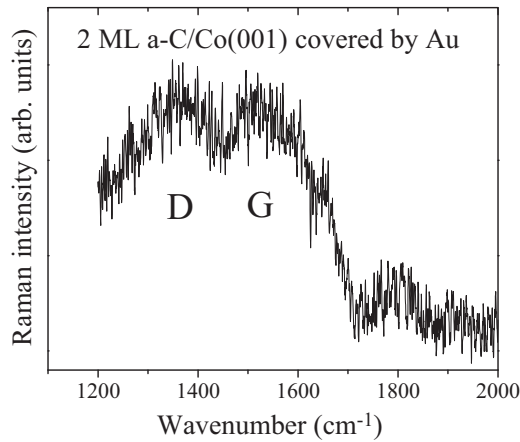


FIG. 5. Raman spectrum of a Au-covered 2 ML a-C film on Co(001). The presence of both peak G (“graphite”) and peak D (“disorder”) is typical of amorphous carbon films.

a maximum around a thickness of 1 ML. As explained in Sec. III B we attribute this behavior to the variation of the CoPc film morphology during deposition, evolving from an incompletely filled to a filled layer for a thickness of 1 ML. The behavior of the spin-motion angles, on the other hand, is quite different. In fact, in the case of ε [Fig. 6(b)] we can identify three thickness regimes. The first regime extends from 0 to 0.28 ML. Here, ε exhibits only very small changes. From 0.28 to about 0.5 ML, we observe a second regime, in which ε breaks down very rapidly. For larger coverages the strongly reduced ε shows only a very slow decrease and vanishes completely for thicknesses above 1 ML. Interestingly, the behavior of ϕ [Fig. 6(c)] is not identical to that of ε . In the first thickness regime below 0.28 ML it shows a significant increase in its absolute value. Although the absolute value of ϕ decreases above 0.28 ML also quite rapidly, the second thickness regime now extends up to about 0.75 ML. For larger coverages ϕ is 0.

The most peculiar feature of the thickness dependence is surely the fact that both spin-motion angles change very abruptly above 0.28 ML. It seems that there exists a sort of threshold value above which the system completely changes its behavior with respect to the reflection of electrons. In the following we investigate the generality of this breakdown phenomenon. This will allow us to rule out several plausible explanations and refine further our problem.

B. Does the breakdown depend on the energy of the primary electrons?

In order to study the effect of the electron energy on the behavior of the reflected electrons, we measured the reflectivity R as well as the electron-spin motion angles ε and ϕ as a function of the CoPc film thickness for different electron energies (see Fig. 7).

Although some details differ with energy (slightly different threshold values, different behavior for thicknesses below the threshold value, additional features at around 0.5 ML), we see that the general behavior as a function of the thickness is quite similar for all studied energies:

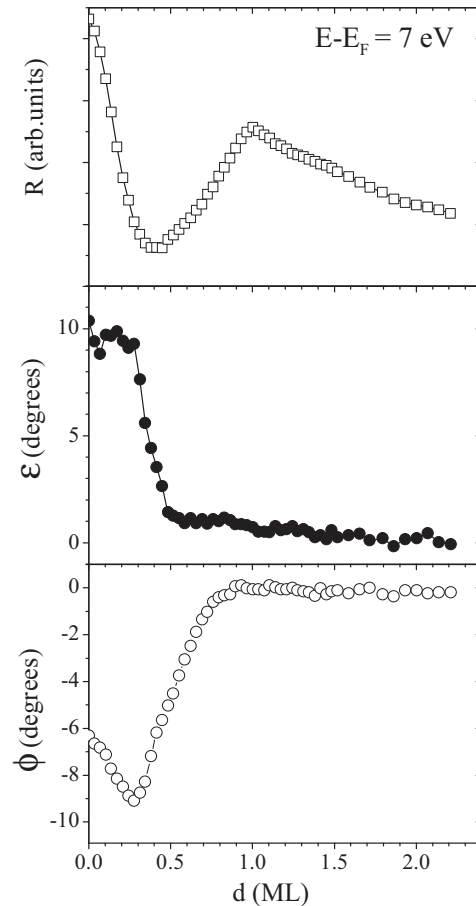


FIG. 6. For the system CoPc/Co/Cu(001), the following quantities are shown as a function of the CoPc film thickness d in monolayers (MLs): spin-averaged electron reflectivity R (top), precession angle ε (middle), and rotation angle ϕ (bottom). The primary electron energy is 7 eV.

(1) There is a threshold value d_1 , above which the absolute values of both spin-motion angles change very strongly. We note at this point that the determination of a small d_1 value is accompanied by a relatively large error. There are two systematic errors which are responsible for this. Besides a certain drift of the evaporation rate during the measurements, the most important source of error is the fact that even when the shutter of the evaporator is closed, molecules always diffuse into the vacuum chamber and thus lead to a very low but non-negligible evaporation rate on the sample surface (verified by Auger spectroscopy).

(2) A very strong change in the spin-motion angles above d_1 up to a thickness of about 0.5 ML is observed. This latter thickness is henceforth called d_2 . A further observation is that this change between d_1 and d_2 is mostly quite linear.

(3) For thicknesses above d_2 two behaviors are observed, depending on the ε or ϕ value reached at d_2 . If the value at d_2 is 0, the measured quantity remains 0. If it is nonzero a decrease in its absolute value is observed, but now on a larger thickness scale.

We note that in the following we continue to call the strong change between d_1 and d_2 “breakdown,” even though the signal

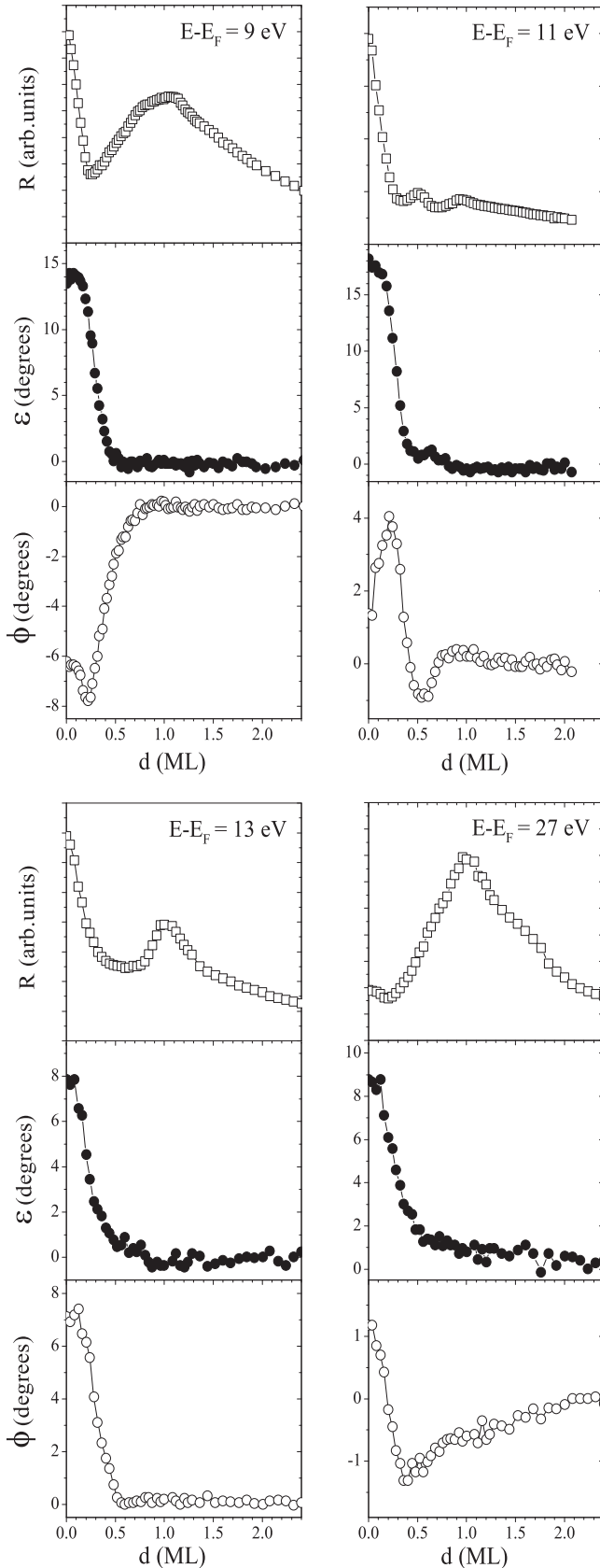


FIG. 7. Spin-averaged electron reflectivity R , precession angle ε , and rotation angle ϕ as a function of CoPc film thickness for four electron energies: 9 eV (top left), 11 eV (top right), 13 eV (bottom left), and 27 eV (bottom right).

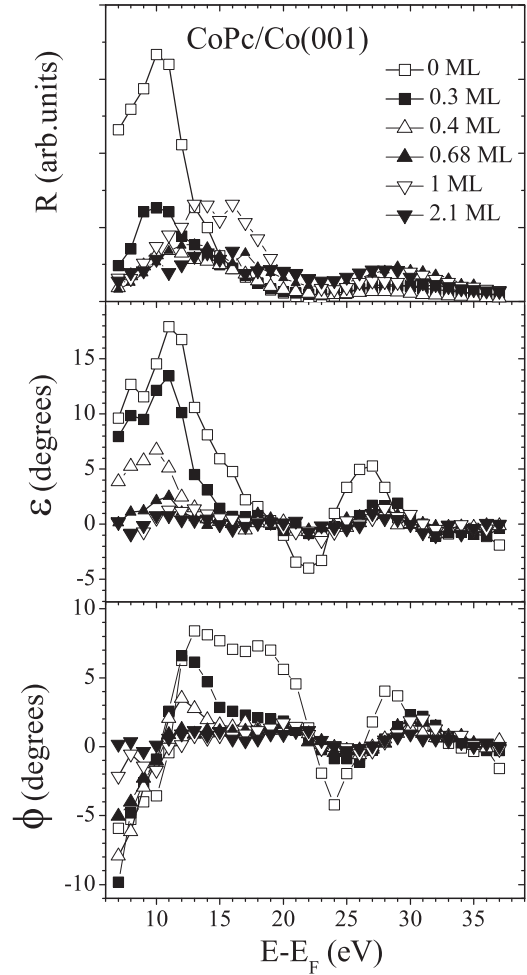


FIG. 8. For the system CoPc/Co/Cu(001), the following quantities as a function of electron energy for different CoPc coverages are shown: spin-averaged electron reflectivity R (top), precession angle ε (middle), and rotation angle ϕ (bottom).

is not quite 0 at d_2 in certain cases (see, for instance, ϕ in Fig. 7, bottom right).

Figure 8 shows the three quantities R , ε , and ϕ as a function of the primary electron energy for several CoPc thicknesses. Although it is of course very difficult, if not impossible, to demonstrate a threshold value for all studied energies, it is clear that both spin-motion angles approach 0 very rapidly. This is an important result, as it shows that the breakdown phenomenon appears for all investigated primary electron energies. This excludes any explanation which is based on the particular electronic band structure of CoPc molecules.

We emphasize that while the spin-motion angles break down in the thickness regime between about 0.2 and 0.5 ML the degree of spin polarization, i.e., the norm of the spin-polarization vector, of the reflected electron beam remains unchanged for all studied thicknesses (see, for instance, Fig. 9 for electrons with a primary energy of 8 eV). Thus, any depolarization of the electron beam during interaction with the CoPc-covered Co surface, for instance, by spin-flip scattering, is excluded.

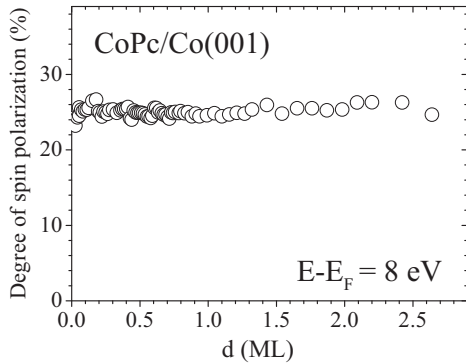


FIG. 9. For the system CoPc/Co/Cu(001) the degree of spin polarization of the reflected electron beam as a function of the CoPc thickness is shown. The primary energy of the electrons is 8 eV.

C. Is the breakdown due to a change in the surface magnetization?

To exclude a possible effect of CoPc molecules on the surface magnetization of Co as the origin of the breakdown, we measured the polarization of secondary electrons as a function of the CoPc thickness. As the spin polarization of the secondary electrons reflects the magnetization state of the ferromagnetic surface, secondary electrons are an ideal probe for this type of study. Figure 10 shows the spin polarization of the complete secondary electron distribution created by unpolarized primary electrons of 132-eV energy. We note that the secondary-electron intensity distribution curve peaks strongly at lower energies such that the contribution of low-energy secondaries dominates the signal. We emphasize that the exponential decay of the signal is as expected. Because of the limited IMFP of the secondary electrons fewer and fewer of them are created in the ferromagnetic substrate, while more and more secondaries are created in the nonmagnetic CoPc layer with increasing CoPc thickness. For thick CoPc coverages we indeed expect to observe zero spin polarization. The essential point of Fig. 10 is that the secondary spin polarization does not exhibit any particular change in the thickness regime

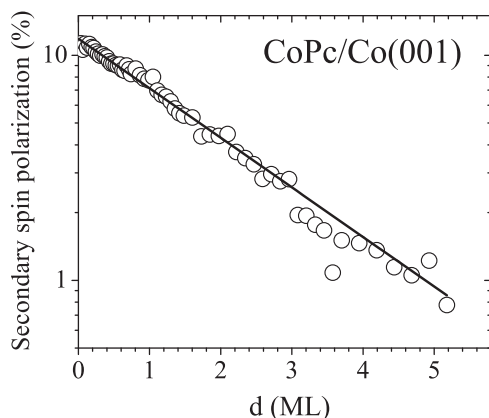


FIG. 10. Spin polarization of secondary electrons as a function of CoPc thickness. The energy of the unpolarized primary electrons is 132 eV. The solid line is a fit to the data based on an exponential decay. Note the logarithmic spin-polarization scale.

where breakdown of the spin-motion angles occurs (between around 0.25 and 0.5 ML). If there were a strong decrease in the surface magnetization in this thickness regime, we would observe a corresponding drop in the secondary-electron spin polarization. As this is not the case, a dramatic change in the Co surface magnetization due to deposition of CoPc in this thickness regime can be excluded. We note that measurements of the x-ray magnetic circular dichroism as well as first-principle calculations give no indication of a dramatic reduction in the Co magnetic moment due to Pc coverage [12]. Finally, we note that situations in which the remanent magnetization becomes 0 or in which the coercive field is larger than the maximum applied magnetic field strength can be excluded. In both cases the measured secondary-electron spin polarization would be 0 or at least strongly reduced.

D. Is the breakdown due to a “mirror” effect?

As phthalocyanine is a semiconductor, it is possible that it leads to an electrical surface charge during the measurement with electrons. In this case, the charging could lead to a “mirror” effect; i.e., the primary electrons are reflected by the CoPc layer without reaching the Co substrate. Therefore, one would not expect any electron spin-motion signal. However, this scenario can be excluded. If there were such an effect, we would (i) not be able to obtain LEED images as shown in Sec. III B and (ii) the primary electrons would not be able to create secondary electrons in the Co substrate. Consequently, the polarization of secondary electrons would be 0, which is not the case (see Fig. 10).

Another fact which excludes the possibility of a mirror effect is that the two spin-motion angles ε and ϕ do not behave in the same manner in several cases [see, for instance, Figs. 6(b) and 6(c)]. While ε is already 0, ϕ is still far from 0. However, in the case of a mirror effect one would expect both spin-motion angles to disappear simultaneously.

In this context we have also studied the work function changes of Co(001) and Cu(001) when covered with Pc by measuring the energy position of the cutoff of the secondary-electron distribution. Work function changes upon molecular adsorption on metal surfaces are caused by a charge transfer between the molecules and the metal substrate, leading to the formation of an interface dipole. Figure 11 shows the work function changes of Co(001) covered by CoPc (top) and Cu(001) covered by MnPc (bottom). In both cases an exponential-like behavior, as expected, with a saturation for coverages above 1 ML is observed. There is no indication that something particular happens with the interface dipole in the thickness regime from 0.25 to 0.5 ML. We note that the work function changes obtained for thick Pc films [-1.1 eV for CoPc/Co(001), -0.9 eV for MnPc/Cu(001)] are in good agreement with measurements on similar systems, which all show values around -1 eV [37–39], and supported by *ab initio* calculations [40].

E. Does the breakdown depend on the choice of the ferromagnetic substrate?

To continue to seek an explanation for this phenomenon, we varied the ferromagnetic substrate using Fe(001) instead of

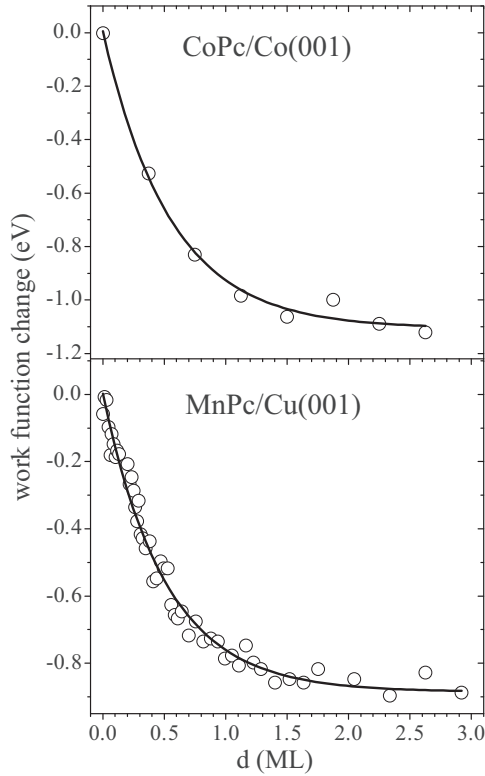


FIG. 11. Work function changes as a function of CoPc thickness on Co(001) (top) and MnPc thickness on Cu(001) (bottom). Lines are exponential fits to the data.

Co(001). We prepared Fe(001) films in two ways, namely, by depositing Fe onto a Ag(001) or onto a Pt(001) single crystal. Figure 12 shows both the spin-averaged electron reflectivity and the spin-motion angles as a function of the CoPc thickness on Fe/Ag(001) (left column) and on Fe/Pt(001) (right column). The strong similarity of the thickness-dependent behavior to that of CoPc films on Co(001) let us immediately conclude that the occurrence of the breakdown phenomenon is independent of the choice of the ferromagnetic substrate.

F. Is the interaction of the molecules with the ferromagnetic substrate of any importance?

Even if a significant effect of the CoPc layer on the strength of the magnetization of Co can be excluded, an influence of CoPc on the spin-dependent electronic band structure of Co due to an interaction between the molecules and the substrate cannot. The latter can, in principle, lead to strong changes in the spin-dependent reflection properties of the Co surface and therefore of the spin-motion angles. However, very recent spin-resolved photoemission experiments performed by some of us as well as calculations performed on MnPc and H₂Pc layers deposited onto Co(001) show, despite the demonstration of strongly spin-polarized molecule-induced interface states, no indications of a significantly changed electronic band structure of Co [12].

To check whether contact of CoPc molecules with the surface of Co is crucial for observing the breakdown phenomenon, we studied a different system. Instead of putting the molecules

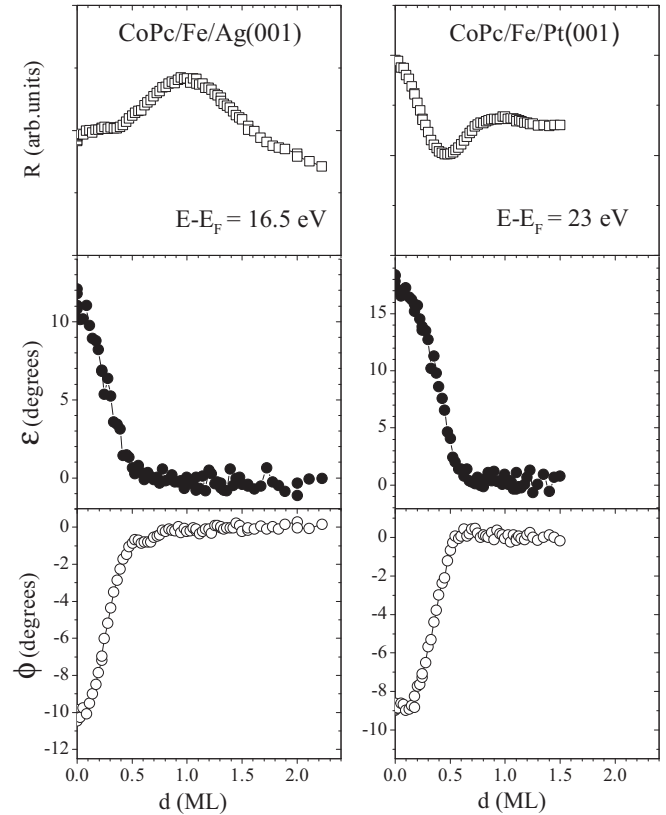


FIG. 12. For the systems CoPc/Fe/Ag(001) (left column) and CoPc/Fe/Pt(001) (right column), the following quantities as a function of CoPc film thickness are shown: spin-averaged electron reflectivity R (top), precession angle ϵ (middle), and rotation angle ϕ (bottom). Primary energies are 16.5 and 23 eV, respectively.

directly on the Co surface, we first deposited a Au film of 9-ML thickness on top of it as an intermediate layer. We have chosen Au, because the IMFP of electrons at low electron energies in Au is quite large [26], such that a significant portion of the detected primary electrons has “seen” the Co/Au interface and thus has experienced an electron-spin motion within the Co substrate even in the presence of a relatively thick Au film.

Figure 13 shows the electron-spin motion angles as a function of CoPc thickness for primary electrons of 8-eV energy. We again observe the same type of behavior as a function of the CoPc thickness: a breakdown of the spin-motion angles above a threshold thickness and the disappearance of both spin-motion angles for thicknesses above 0.5 ML. Moreover, the values of d_1 and d_2 are very close to those obtained with CoPc directly deposited onto the Co surface. Further experiments with an even thicker intermediate Au layer of 15 ML give a similar result (see Fig. 14). The fact that it is not necessary to have any direct contact of the molecules with the ferromagnetic substrate to obtain the breakdown of the spin-motion signal is surely the most surprising result. We note that only Au in immediate contact with a ferromagnetic substrate, i.e., the first Au layer, can be polarized. But even in this case the induced magnetization in Au is very small [41] ($0.03 \mu_B/\text{atom}$). Consequently, the nonmagnetic molecules cannot possess any induced magnetization when they are separated from the ferromagnetic substrate by an

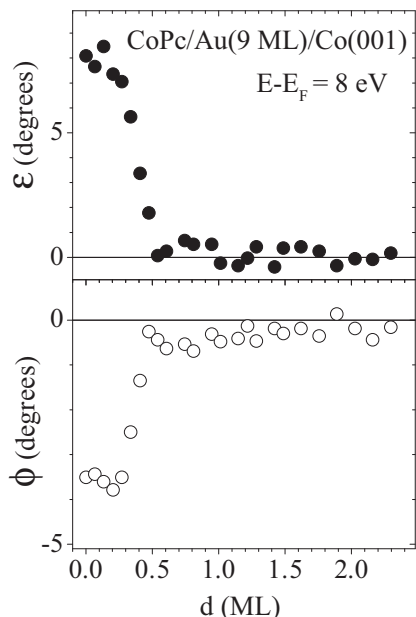


FIG. 13. For the system CoPc/Au(9ML)/Co/Cu(001), the spin-motion angles ε (top) and ϕ (bottom) are shown as a function of the CoPc coverage. The primary energy is 8 eV.

intermediate Au layer as thick as 15 ML. We note for the sake of completeness that molecules deposited directly onto the nonmagnetic Cu(001) substrate surface do not exhibit any spin-motion signal.

G. Does the breakdown depend on the choice of the organic molecule?

To investigate the generality of the breakdown phenomenon, we studied different types of organic molecules:

- (a) different phthalocyanines with a varying central metal ion, in order to test the possible role of the latter—CoPc, FePc, MnPc, and H₂Pc;
- (b) other aromatic molecules such as PTCDA (containing, besides carbon and hydrogen, also oxygen) and coronene (containing only carbon and hydrogen);
- (c) the nonplanar molecule C₆₀ (as C-H bonds do not exist in C₆₀, their possible role can be tested);

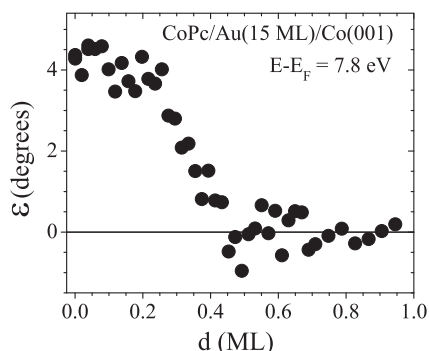


FIG. 14. For the system CoPc/Au(15ML)/Co/Cu(001), the precession angle ε as a function of the CoPc coverage is shown. The primary energy is 7.8 eV.

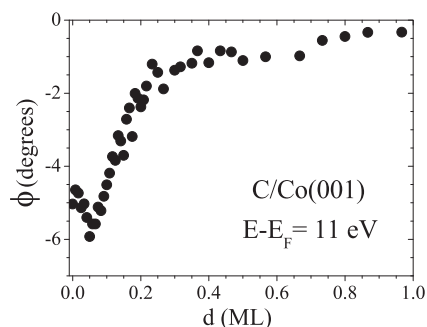


FIG. 15. For the system C/Co/Cu(001) the rotation angle ϕ as a function of the C coverage is shown. The primary energy is 11 eV.

(d) the alkane pentacontane, in which the carbon atoms are exclusively bonded by single bonds, in order to test the possible role of the aromaticity of the organic molecules in (1)–(3);

(e) and, finally, pure a-C.

As in the first considered case, namely, CoPc, we deposited several molecule species not only directly onto a ferromagnetic substrate but also onto an intermediate Au layer in order to decouple the molecules from the ferromagnetic substrate. In all cases, i.e., for all molecules as well as a-C (see Fig. 15), in direct contact or not with the ferromagnetic substrate, a very similar behavior as a function of thickness is observed. In particular, the presence of three coverage regimes determined by the thicknesses d_1 and d_2 is found for any choice of the molecule species. Figure 16 shows, for instance, the negative rotation angle $-\phi$ as a function of the pentacontane thickness. This nice example shows both the beginning (at d_1) and the end (at d_2) of the breakdown of $-\phi$ in a very clear manner. In fact, from this logarithmic plot it becomes clear that after the strong decay that ends at about 0.45 ML, the further decrease in $-\phi$ follows an usual exponential behavior.

It can be concluded that the existence of the breakdown phenomenon does not depend at all on the precise structure and composition of the organic molecule. It seems to be the mere presence of carbon atoms (independent of their

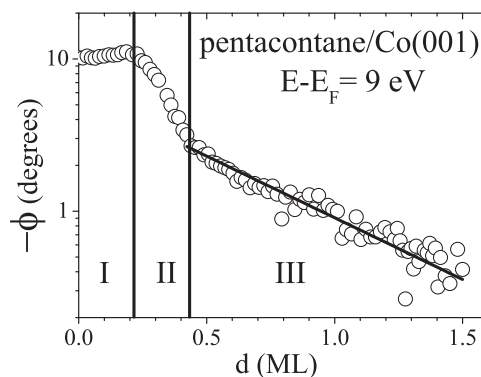


FIG. 16. For the system pentacontane/Co/Cu(001) the negative rotation angle $-\phi$ as a function of the pentacontane thickness is shown. The primary energy is 9 eV. The three thickness regimes are indicated. Note the logarithmic $-\phi$ scale. The line is an exponential fit to the data in thickness regime III.

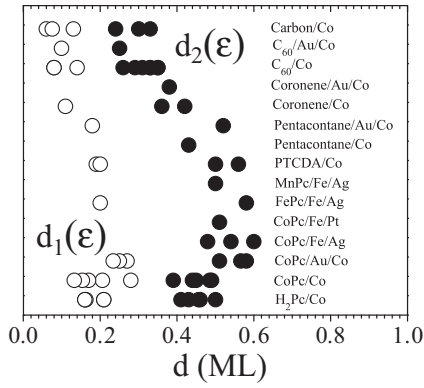


FIG. 17. Thicknesses d_1 and d_2 obtained from measurements of the precession angle ϵ .

state of hybridization) that is the essential ingredient for the breakdown phenomenon.

We note that the presence of the breakdown phenomenon for C_{60} excludes any relationship between the latter and the so-called organic magnetoresistance (OMAR) [42]. The absence of OMAR in C_{60} -based systems, which was shown by Nguyen *et al.* [43], clearly shows that hydrogen (not present in C_{60}), resulting in a hyperfine coupling induced by the protons' nuclear spins, is a necessary prerequisite for the observation of OMAR.

Figures 17 and 18 show the thicknesses d_1 and d_2 for all studied systems and energies. We note that the determination of the thickness d_1 , apart from the problems mentioned in Sec. IV B, is particular difficult in certain cases. Whether its determination is easy or difficult depends on the manner in which the measured quantity (ϵ or ϕ) varies at the beginning. If the absolute value of the quantity decreases as a function of thickness it becomes very difficult or even impossible to identify a threshold. However, for situations for which the absolute value of the quantity remains constant or even increases, the threshold value d_1 is well defined.

The fact that the breakdown phenomenon saturates at d_2 values which are much smaller than 1 ML is a quite astonishing result, because most of the ferromagnetic surface is still available for electron scattering. Should we not expect to have saturation for a completed ML instead? One can

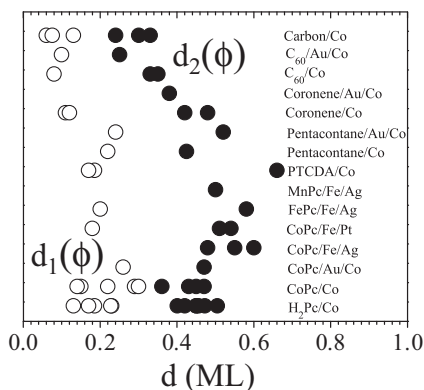


FIG. 18. Thicknesses d_1 and d_2 obtained from measurements of the rotation angle ϕ .

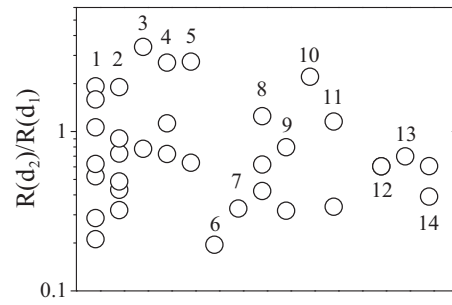


FIG. 19. The ratio $R(d_2)/R(d_1)$ for (1) H_2Pc/Co , (2) $CoPc/Co$, (3) $CoPc/Au/Co$, (4) $CoPc/Fe/Ag$, (5) $CoPc/Fe/Pt$, (6) $FePc/Fe/Ag$, (7) $MnPc/Fe/Ag$, (8) $PTCDA/Co$, (9) pentacontane/ Co , (10) pentacontane/ Au/Co , (11) coronene/ Co , (12) C_{60}/Co , (13) $C_{60}/Au/Co$, and (14) C/Co . Note the logarithmic scale of the ordinate.

understand such a low saturation value if we hypothesize that the molecules or the carbon islands appear much larger for the reflected electrons; i.e., they have a cross section which is larger than the “actual” size of the molecules or carbon islands. As mentioned before, one might expect saturation of the effect for a completed ML. If we apply this to the (hypothetically) enlarged cross section of the molecules or carbon islands, we must conclude that the cross section has to be about two to three times larger than the “actual” size of the molecules or carbon islands; i.e., it seems that the molecules or carbon islands possess a relatively large influence zone that affects the spin-dependent scattering of electrons.

We emphasize at this point that the breakdown phenomenon which is observed for all studied systems is not seen in the behavior of the reflected intensity as a function of the thickness. In fact, considering all data no clear relationship between reflectivity and spin-motion angles is found. In the interesting thickness range between d_1 and d_2 the reflectivity shows all sort of behavior: a weak or strong increase, a weak or strong decrease, or even nonmonotonous behavior. In order to express these different behaviors with a single quantity we have calculated the ratio $R(d_2)/R(d_1)$ of the reflectivities for the coverages d_2 and d_1 . The ratio is plotted in Fig. 19 and it varies between 0.2 and 4. Of particular importance is the fact that some data exist which have a ratio close to 1; i.e., the reflected intensities in these cases are the same at d_1 and d_2 , while the spin-motion angles are not.

In the following we suggest that the appearance of the breakdown phenomenon depends on the average carbon surface density in each system. In order to find out whether this hypothesis is consistent with our data we have to know the average carbon surface density σ_C^{ML} for a complete ML (see Table I). When data were not available in the literature, the σ_C^{ML} of a similar system was taken. For molecules on $Co(001)$ we took the same values as for molecules on $Cu(001)$.

By multiplying the average carbon surface density σ_C^{ML} for a completed ML by the thickness d_2 expressed in units of ML, we obtain directly the average carbon surface density that is obtained at the end of the breakdown (see Fig. 20). For the planar molecules Pc, PTCDA, pentacontane, and coronene on $Co(001)$, $Fe(001)$, or $Au(111)/Co(001)$, as well as carbon on $Co(001)$, we obtain very similar values: $d_2 \cdot \sigma_C^{ML} = 9 \pm 2 \text{ nm}^{-2}$. The situation is quite different for C_{60} , for which

TABLE I. Average carbon surface density σ_C^{ML} of a completed ML as number of carbon atoms per nm^2 . In the case of C_{60} it is the projected average carbon density on the surface.

System	σ_C^{ML} [Ref. No.]
Pc/Cu(001)	17 [27]
Pc/Au(111)	14 [44]
PTCDA/Cu(001)	18 [45]
$\text{C}_{44}\text{H}_{90}$ /Cu(001)	15 [46]
$\text{C}_{30}\text{H}_{62}$ /Au(111)	15 [47]
Coronene/Cu(001)	26 [45]
Coronene/Ag(111)	21 [48]
C_{60} /Cu(001)	60 [49]
C_{60} /Au(111)	69 [50]
Graphite	38

$d_2 \cdot \sigma_C^{\text{ML}}$ is about two times larger than for the planar molecules and carbon. It seems that only one half of the carbon atoms contributes to the breakdown phenomenon in C_{60} .

1. A percolation analysis

Additional interesting information might be obtained from the fact that the breakdown phenomenon presents a threshold thickness d_1 . The presence of a threshold is often typical of the onset of a percolation process. This leads us to think that the breakdown phenomenon is related to the long-range connectivity of the (hypothetically) enlarged cross sections of the molecules. In order to corroborate this supposition we performed kinetic Monte Carlo simulations of the deposition of particles on an fcc (001) surface with $N \times N$ surface sites. The locations of the deposited particles are chosen randomly. The ML is defined as the deposition of N^2 particles.

The connectivity between particles strongly depends on their ability to diffuse on the surface: the stronger the diffusion, the more compact the deposited layer and the larger the critical percolation thickness. It is therefore crucial to characterize the diffusion behavior of the particles on the surface before performing any percolation analysis. To determine the diffusion conditions we compared STM images with kinetic Monte Carlo simulations. Figure 21(a) displays an STM image ($40 \times 40 \text{ nm}^2$) recorded at 4 K of 0.3 ML of room-temperature deposited MnPc on a Co(001)

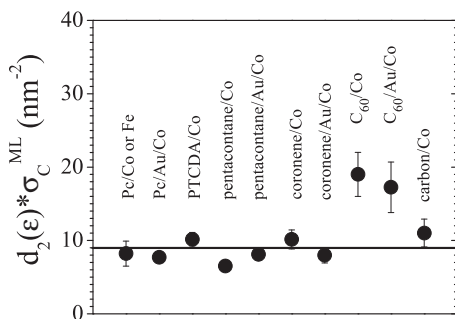


FIG. 20. The product of d_2 and the average carbon surface density σ_C^{ML} of a completed ML is shown for all systems studied. In the case of C_{60} it is the projected average carbon density on the surface.

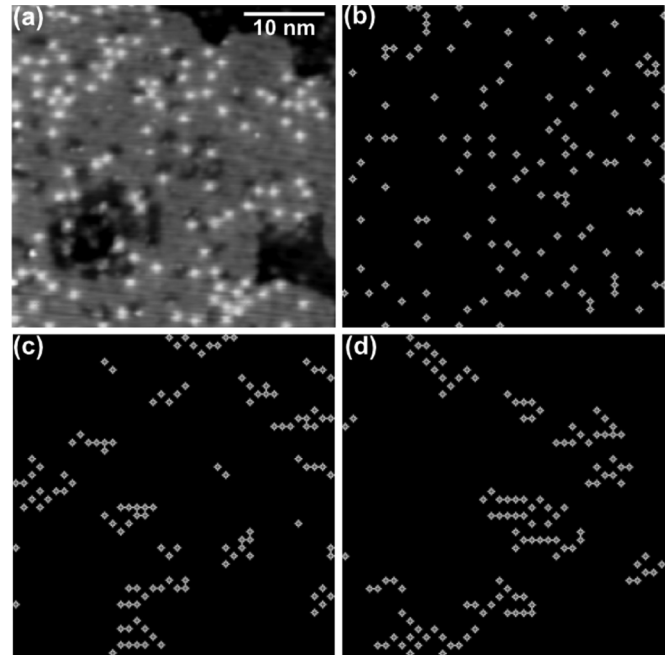


FIG. 21. (a) STM image ($40 \times 40 \text{ nm}^2$) taken at 4 K of 0.3 ML of MnPc deposited at room temperature onto a Co(001) film. (b–d) Kinetic Monte Carlo simulations of the deposition without any diffusion (b), with diffusion by one lattice step of particles which arrive at the surface during a deposition step (c), and with diffusion by one lattice step of all particles at each step of the deposition (d). Particles in (c) and (d) which become or are part of a cluster are not allowed to diffuse anymore.

film. The molecules are the bright spots in the figure. Figures 21(b)–21(d) display three simulations in which particles are deposited onto a substrate with 40×40 surface sites. While no diffusion is allowed in Fig. 21(b), Fig. 21(c) displays a situation for which only particles arriving at the surface during a deposition step are allowed to move by one lattice position. In Fig. 21(d) all particles are allowed to move at each deposition step by one lattice position. However, particles in Figs. 21(c) and 21(d) which become or are already part of a cluster are not allowed to diffuse anymore.

Comparison of the simulations with Fig. 21(a) shows that the best agreement is obtained for the situation displayed in Fig. 21(c). When diffusion is suppressed, there are too many isolated particles [Fig. 21(b)], whereas full diffusion leads to their absence [Fig. 21(d)].

Having worked out the question of the molecular diffusion, we now turn to the key issue of the connectivity between particles. Figure 22 displays both experimental data and the simulated percentage of nonpercolated sites (NP) as a function of the thickness. A particle is considered to be percolated if it belongs to a cluster spanning the substrate. In order to compare the simulations with the experimental data the thickness scale of the latter has to be multiplied by a factor which is given by the different surface areas that are occupied by 1 ML of molecules in the experiments (64%) [44] and 1 ML of particles in the simulations (100%).

Figure 22 displays average curves (of 20 simulations) supposing three different situations. In simulation 1, for which no further influence zone around the particles is supposed (see

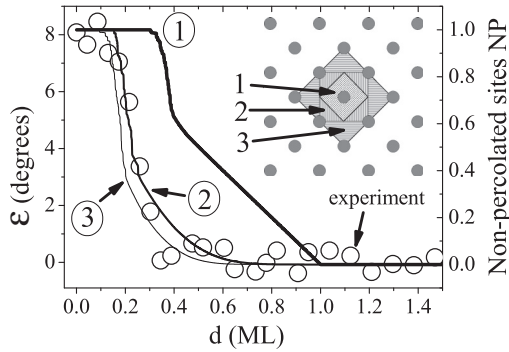


FIG. 22. Both the experimental obtained precession angle ε (for the system CoPc/Au/Co; open circles) and the simulated percentage of nonpercolated sites (NP; lines) are shown as a function of the thickness. Note that the thickness scale of the experimental data is multiplied by a factor of 0.64 (see text). Simulations are shown for three situations: Situation 1 corresponds to the pure (square) particle. In situation 2 the influence zone is given by the particle plus a zone determined by the nearest-neighbor positions. In situation 3 the influence zone is given by the particle plus a zone determined by the nearest- and next-nearest-neighbor positions. Inset: Surface lattice and geometry of the three situations considered here.

situation 1 in the inset in Fig. 22), two particles are considered to be connected when they are nearest neighbors. In the early stages of the deposition NP is 1, indicating that there is no percolated cluster present on the surface. At about 0.32 ML a quite rapid change in NP is observed, a behavior which is typical of a percolation process indicating the percolation threshold. From 0.4 ML on, each newly deposited particle will be in contact with a percolated cluster, thus leading to a linear decrease in NP down to 0 until the film is completed at 1 ML.

By comparing simulation 1 with the experimental values for CoPc/Au/Co (open circles in Fig. 22), we see that both the threshold d_1 and the saturation d_2 are much larger in the simulation. A much better agreement with experiment is only obtained by supposing the existence of an influence zone around each particle that influences the spin-dependent electron reflection. In simulation 2 this zone is composed of the shell of the nearest-neighbor positions (leading to a doubling of the cross section compared to the particle's surface; see situation 2 in the inset in Fig. 22), while in simulation 3 the shells of both the nearest-neighbor and the next-nearest-neighbor positions are included (leading to a quadrupling of the cross section compared to the particle's surface; see situation 3 in the inset in Fig. 22). Thus, the kinetic Monte Carlo simulations give strong support for the existence of a region around the molecules that influences the spin dependence of the electron reflectivity.

2. Do elements other than carbon exhibit the breakdown phenomenon?

One might wonder now if any element other than carbon is able to induce the same type of breakdown of the spin-motion angles. Of course, we are not able to make a systematic study of the whole periodic system. However, certain experiments which have been performed in the past by several of us as well as by other groups indicate that the following elements

do not show this behavior: Au [26], Cu [28], Ag [51], Pd [51], Mn [52], Cr [53], V [54], Pb [55], Mg [55], and O [56]. In these experiments either the spin-motion angles or the exchange asymmetry, being closely related to the rotation angle ϕ , were measured. Experiments with Si, which is isoelectronic to C, were not performed but probably would not have been conclusive because of the strong tendency of Si to alloy with the ferromagnetic transition metals, at least at room temperature. Experiments at low temperatures, which are not possible with the present setup, might be interesting. We speculate, however, that the compound boron nitride (BN), which is also isoelectronic to carbon, might be a candidate.

Another interesting question is whether organic molecular magnets exhibit the breakdown phenomenon. Will the presence of carbon atoms in the molecules lead to the breakdown of the spin dependence of the electron reflectivity, which is created by exactly the same molecules?

H. Does the breakdown depend on the orientation of the initial spin polarization?

In all experiments presented up to now we have studied the spin-motion angles for which the initial spin polarization \mathbf{P}_0 was aligned perpendicularly with respect to the magnetization \mathbf{M} . Furthermore, in all cases \mathbf{P}_0 was also oriented perpendicularly with respect to the scattering plane. In order to test whether the orientation of \mathbf{P}_0 with respect to the scattering plane has any importance for the breakdown phenomenon we performed an experiment in which \mathbf{P}_0 lay in the scattering plane (see inset in Fig. 23). Figure 23 shows, for the case of PTCDA/Co(001), ε as a function of the PTCDA thickness for both orientations of \mathbf{P}_0 . As the thickness dependencies are very similar, in particular, with the same values for d_1 and d_2 , the orientation of \mathbf{P}_0 obviously has no influence on the breakdown phenomenon. We note that the fact that the breakdown phenomenon is independent of the orientation of \mathbf{P}_0 excludes any explanation based on the possible existence of persistent ring currents in the aromatic cycles. A magnetic field produced by such a current would be oriented perpendicularly with respect to the surface and should therefore lead to different effects depending on the orientation of the initial polarization.

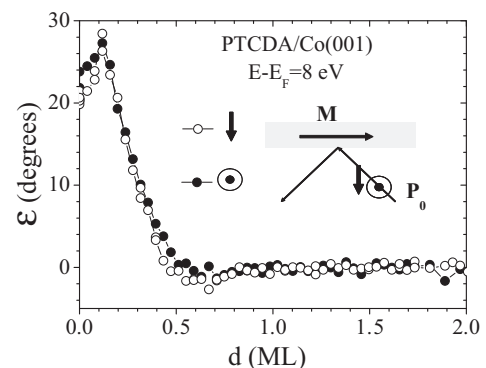


FIG. 23. For the system PTCDA/Co/Cu(001) the precession angle ε as a function of the PTCDA thickness is shown for two orientations of the initial spin polarization \mathbf{P}_0 . The primary energy of the electrons is 8 eV.

At any rate, the breakdown phenomenon is also seen with linear chains of alkanes in which persistent ring currents cannot exist.

What happens if we orient \mathbf{P}_0 not perpendicularly with respect to the magnetization direction, but parallel or antiparallel to it? In this case, of course, we will not be able to measure any spin motion. However, we can measure the so-called exchange asymmetry (normalized to the initial spin polarization P_0)

$$A_{\text{ex}} = \frac{1}{P_0} \frac{R^{\uparrow\uparrow} - R^{\uparrow\downarrow}}{R^{\uparrow\uparrow} + R^{\uparrow\downarrow}},$$

where $R^{\uparrow\uparrow}$ and $R^{\uparrow\downarrow}$ are the reflected electron intensities with \mathbf{P}_0 parallel and antiparallel to \mathbf{M} , respectively. If we take into account that the intensities $R^{\uparrow\uparrow}$ and $R^{\uparrow\downarrow}$ are proportional to the quantities $|r^{\uparrow\uparrow}|^2$ and $|r^{\uparrow\downarrow}|^2$, respectively, which we introduced in Sec. II, we can directly identify the asymmetry

$$A = \frac{1}{P_0} \frac{|r^{\uparrow\uparrow}|^2 - |r^{\uparrow\downarrow}|^2}{|r^{\uparrow\uparrow}|^2 + |r^{\uparrow\downarrow}|^2}$$

with the exchange asymmetry A_{ex} . As A and the rotation angle ϕ are closely related, we thus expect the same type of breakdown phenomenon also for A_{ex} . Figure 24 shows the exchange asymmetry A_{ex} as a function of the FePc thickness on Fe(001). Indeed, A_{ex} behaves similarly as in the perpendicular spin configurations and exhibits the breakdown phenomenon.

Finally, we consider the configuration for which \mathbf{P}_0 is 0. The only quantity which we can measure in this case is the spin polarization, which is created due to the spin-dependent reflection of the electrons at the surface of the ferromagnetic substrate. As elastic exchange scattering, responsible for spin flips, can be neglected [57], the spin polarization P created with an unpolarized electron beam should be identical to the exchange asymmetry A_{ex} created with a (completely) polarized electron beam, $P = A_{\text{ex}}$. As A_{ex} exhibits the breakdown phenomenon, we expect the same behavior for P . In fact, this is exactly what we observe, for instance, for the system $\text{C}_{60}/\text{Co}(001)$ in Fig. 25.

I. Does the breakdown concern only elastically scattered electrons?

Up to now we have studied the breakdown effect on elastically scattered primary electrons. In order to find out

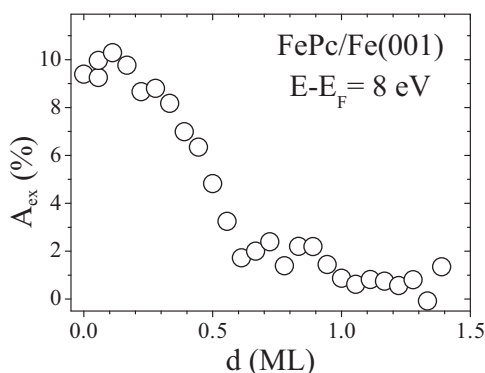


FIG. 24. For the system FePc/Fe(001) the exchange asymmetry A_{ex} as a function of the FePc thickness is shown. The primary energy of the electrons is 8 eV.

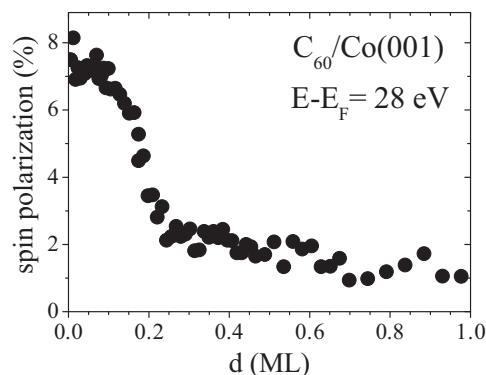


FIG. 25. For the system $\text{C}_{60}/\text{Co}/\text{Cu}(001)$ the degree of spin polarization of the reflected electron beam as a function of the C_{60} thickness is shown. The initial spin polarization is 0. The primary energy of the electrons is 28 eV.

whether all primary electrons, being elastically or inelastically scattered, are subject to this effect, we performed two types of measurements. In the first experiment electrons leaving the sample are detected in the spin detector. For this experiment the retardation grid of the energy analyzer was set to 0 such that all electrons scattered within the angular acceptance angle of the energy analyzer of a few degrees, independent of their loss in energy, are detected. The incident electrons are unpolarized. Figure 26 shows the spin polarization of the detected electrons as a function of the CoPc thickness on Co(001) for two primary energies, 132 and 26.5 eV, and taken in off-specular geometry (by 5°). In the case of 132 eV the spin polarization shows an exponential decay, while that for 26.5 eV exhibits a change of slope around 0.5 ML. In order to understand this difference between these two primary energies, we have to know which electronic distributions are formed during interaction of the incoming electron beam with the sample. There are three contributions: (i) elastically scattered primary electrons, (ii) inelastically scattered primary electrons, and (iii) secondary electrons. As we have detected the scattered electrons in off-specular geometry, the contribution of elastically scattered primaries to the measured signal is very small. Thus, the spin

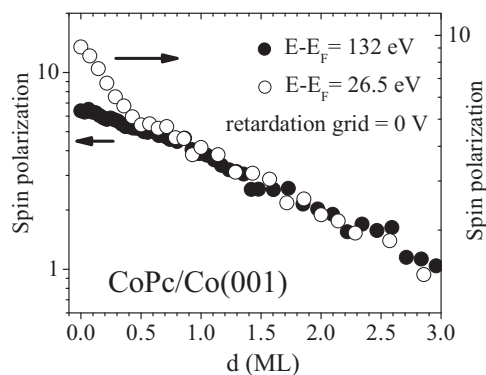


FIG. 26. For the system $\text{CoPc}/\text{Co}/\text{Cu}(001)$ the degree of spin polarization of inelastic electrons (both inelastically scattered primaries and secondaries), taken in off-specular geometry (by 5°), as a function of the CoPc thickness is shown. Primary energies of the unpolarized incident electrons are 26.5 and 132 eV.

polarization P in Fig. 26 consists of only two contributions, namely, that of inelastically scattered primaries and that of secondaries,

$$P = \frac{P_{ip} \cdot I_{ip} + P_{sec} \cdot I_{sec}}{I_{ip} + I_{sec}},$$

with P_{ip} and I_{ip} the spin polarization and the intensity of the inelastically scattered primaries, respectively, and P_{sec} and I_{sec} the spin polarization and intensity of the secondaries, respectively.

The key to understanding the difference between the signals for 132 and 26.5 eV is the fact that the number of secondaries increases strongly with increasing primary energy and can be much higher than the number of incoming primaries, while the number of inelastically scattered primaries can never be larger than that of incoming primaries. Consequently, for 132 eV the contribution of secondary electrons dominates the signal, such that the contribution of inelastically scattered primary electrons can be neglected. The situation is quite different for 26.5 eV. As the energy of the incoming primaries is now much lower, the number of secondaries is strongly reduced with respect to the situation at 132 eV (by one order of magnitude) and becomes comparable to the number of inelastically scattered primaries. The change in slope for 26.5 eV can now be explained if we assume that the inelastically scattered primary electrons are subject to the breakdown phenomenon, leading to the same d_2 value (of about 0.5 ML) as for the elastically scattered primaries. For thicknesses larger than d_2 the inelastically scattered primaries still contribute to the total intensity, $I_{ip} + I_{sec}$, but as their spin polarization P_{ip} is now 0 or at least strongly reduced, the total spin polarization P is significantly smaller.

In the second experiment the absorbed sample currents $I_a^{\uparrow\uparrow}$ and $I_a^{\uparrow\downarrow}$, with \mathbf{P}_0 parallel and antiparallel to \mathbf{M} , respectively, are measured. In this way we obtain the spin asymmetry of the absorbed sample current (normalized to the initial spin polarization):

$$A_a = \frac{1}{P_0} \frac{I_a^{\uparrow\uparrow} - I_a^{\uparrow\downarrow}}{I_a^{\uparrow\uparrow} + I_a^{\uparrow\downarrow}}.$$

We note that the absorbed current I_a is complementary to the total reflected current I_r , i.e., $I_a = I_0 - I_r$, with I_0 the electron current arriving from the GaAs electron source. By measuring A_a we therefore have access to the spin asymmetry of the total reflected current, which is the simple sum of the elastically reflected current, being the sum of the LEED beam intensities [not just of the specular (00) beam], and the inelastically reflected current, which accounts for all electrons reflected with energies lower than the primary energy and at arbitrary angles. Thus, any change in the spin asymmetry of the total reflected current must lead to a complementary change in A_a . The magnitudes of these two asymmetries are simply related by the ratio of the coefficients for reflection and absorption [58]. Figure 27 shows the negative spin asymmetry of the absorbed sample current $-A_a$ and, for comparison, the spin asymmetry of the (00) beam $A_{(00)}$ as a function of the CoPc thickness for the system CoPc/Co(001). We note that the relatively low primary energy of 13 eV was chosen in order to keep the contribution of secondary electrons to the current

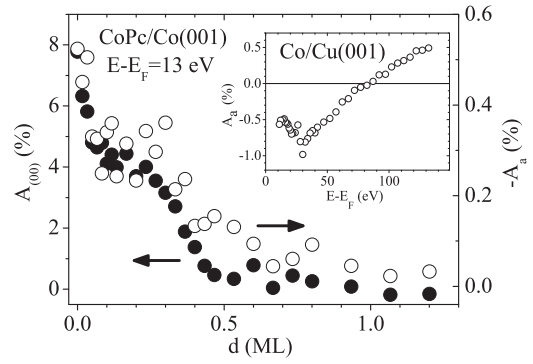


FIG. 27. For the system CoPc/Co/Cu(001) both the asymmetry of the (00) beam $A_{(00)}$ and the negative asymmetry of the absorbed sample current $-A_a$ as a function of the CoPc thickness are shown. The primary energy of the electrons is 13 eV. Inset: Asymmetry A_a of an uncovered Co film as a function of the electron energy.

leaving the sample small. The essential point is that $-A_a$ and $A_{(00)}$ exhibit very similar behavior. This proves that the breakdown phenomenon which is observed for the (00) beam is also present when we consider the total reflected current. We emphasize that the contribution of the elastically scattered electrons to the total reflected current is small so that the inelastically scattered electrons dominate the total reflected current.

We note that as coherence does not exist between the inelastically scattered electrons, any explanation of the breakdown phenomenon in terms of coherent electrons can be excluded.

J. Does the breakdown phenomenon influence the spin-dependent electron transmission?

While studying the effect on the absorbed sample current, we realized that this type of experiment might also give an answer to another question, namely, whether the breakdown phenomenon which appears in reflection geometry also influences the spin-dependent transmission properties of electrons. As we cannot do experiments with freestanding layers, in the following we exploit the spin filtering effect in ferromagnetic materials as a probe to study the transmission of electrons across the molecular layers.

Let us first observe carefully the inset in Fig. 27. It shows the asymmetry A_a for a pure uncovered Co(001) film as a function of the electron energy. By increasing the electron energy (up to 130 eV) we observe that the asymmetry changes sign at around 80 eV and remains positive for higher energies. To understand this behavior we first have to emphasize that the total reflected current, which is complementary to the absorbed current, consists, in general, of elastically and inelastically scattered primary electrons as well as secondary electrons. However, at high electron energies the contribution of secondary electrons dominates so that the contribution of primary electrons can be neglected. The change in sign of A_a is now understood in the following way. Because of the spin asymmetry of the IMFP of the electrons in the ferromagnetic Co film, i.e., the spin filtering effect, the primary electrons are subject to a different number of collisions across the ferromagnetic layer, depending on whether the spin is a majority spin or a minority spin. Consequently, majority-spin and minority-spin primary

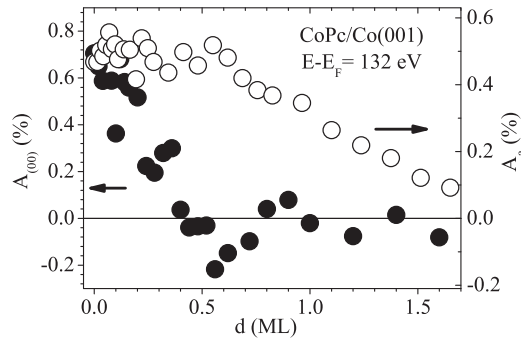


FIG. 28. For the system CoPc/Co/Cu(001) both the asymmetry of the (00) beam $A_{(00)}$ and the asymmetry of the absorbed sample current A_a as a function of the CoPc thickness are shown. The primary energy of the electrons is 132 eV.

electrons create different numbers of secondary electrons. As majority-spin electrons have a longer IMFP than minority-spin electrons [59], the latter create more secondary electrons and therefore lead to a smaller I_a value, i.e., a positive value of A_a . We therefore understood that measuring the absorbed current at high electron energies could be a way to determine whether or not the spin-filter effect and thus the spin-dependent transmission within the ferromagnetic film is influenced by the deposition of organic molecules.

The same type of experiment as described before was therefore performed at the much higher primary-electron energy of 132 eV. Figure 28 shows the asymmetry A_a and, for comparison, the asymmetry of the (00) beam $A_{(00)}$ as a function of the CoPc thickness for the system CoPc/Co(001). While $A_{(00)}$ exhibits a clear breakdown as also observed for much lower electron energies (see Fig. 27), A_a behaves quite differently, as it varies only little and does not show a breakdown of the signal in the thickness range where this is observed for elastic electrons. The essential point is that the presence of the organic layer obviously has no particular effect on the spin filtering properties within the ferromagnetic film, i.e., on the spin-dependent transmission properties, while the spin-dependent reflection properties are strongly influenced. In particular, the spin of the incident electrons which traverse the interface and then continue their path within the ferromagnetic material is not significantly influenced. The exponential decrease in A_a with increasing CoPc thickness, which is observed for coverages above 0.5 ML, on the other hand, is as expected, as CoPc does not exhibit spin dependence of the IMFP such that the production of the secondary electrons becomes spin independent for large CoPc thicknesses.

K. Does a buried organic film behave differently?

We have seen in the preceding sections that the deposition of organic molecules or carbon has a dramatic effect on the spin-motion angles as well as on related quantities. The fact that the breakdown phenomenon appears even in film systems in which the ferromagnetic substrate and the organic or carbon layer are well separated from each other let us suppose that the behavior of the interface vacuum/organic layer is of crucial importance for understanding the breakdown phenomenon. One might wonder therefore whether a modification of this

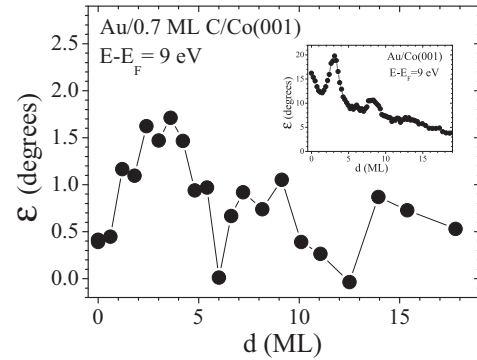


FIG. 29. For the system Au/0.7 ML C/Co(001), the precession angle ϵ as a function of the Au coverage is shown. The primary energy is 9 eV. Inset: ϵ as a function of Au coverage on top of Co(001).

interface could lead to a different behavior. In this vein we studied the spin-motion angles as a function of Au deposition on top of a Co(001) film covered with 0.7 ML of carbon (see Fig. 29). Because of the breakdown phenomenon the ϵ signal after deposition of 0.7 ML carbon is only 0.5° , while the starting signal before C deposition is 16° . In the second step Au was deposited on this system. Interestingly, deposition of Au, which leads to reflection conditions at the Au/C interface that are quite different from those at the vacuum/C interface, does not result in a “recovery” of the ϵ signal. Instead the small signal is only modulated by the Au deposition in a way similar to Au deposition on Co(001) (see inset in Fig. 29). In the past these oscillations have been explained in terms of quantum-well states within the Au(111) layer [26]. We note that similar experiments have been performed also with Pc molecules. As in the above-described experiments with C no “recovery” of the spin-motion signal could be observed during deposition of Au.

L. Do spin-motion first-principle calculations predict the breakdown phenomenon?

In order to unravel the physical origin behind the breakdown phenomenon we performed spin-motion first-principle calculations on carbon-covered Fe(001) films using the linear muffin-tin orbital method (LMTO) [60,61] to determine the self-consistent potentials. These potentials are then used in the layered Korringa-Kohn-Rostoker (LKRR) method [62–66] to compute the spin-polarized low-energy electron diffraction [66] (SPLEED). The theory of SPLEED is well documented in the literature [66–68]. To summarize, an incident electron beam, generated by a source of polarized electrons, of kinetic energy E , wave vector \mathbf{k} , and spin polarization vector \mathbf{P} , is reflected by a surface as a low-energy diffracted electron with energy $E' = E$, wave vector \mathbf{k}' , and spin polarization \mathbf{P}' . The main idea behind SPLEED is to use the multiple scattering method to compute the intensity and spin polarization \mathbf{P}' of the reflected electrons. The first step in multiple scattering theory is to determine the scattering properties by a single-site t matrix. One then has to compute the scattering properties of a single layer by means of the LKRR method. To compute the scattering properties of an arbitrary stack of layers, one first computes the scattering properties of a double layer. After

n iterations the scattering matrix of 2^n layers is obtained. The reflected electron beam intensity and spin polarization are then obtained from the total reflection matrix of the entire semi-infinite system, which in turn is determined from the scattering matrix [66,67]. We note that the same type of calculations was performed recently by us, using the so-called OMNI2K code developed by Henk [68] for MgO films on Fe(001) [69] and Fe(001) films on Ag(001) [70]. The computed angles of the spin polarization showed reasonable agreement with the experimental results and allowed us to understand the particular behavior we observed in these experiments.

Two systems are investigated: 9 ML Fe(001) and 1 ML C on 9 ML Fe(001). As 1 ML is much larger than the thickness d_2 of C (about 0.25 ML), which we found in our experiments, we expect the complete disappearance of the spin-motion angles for Fe covered with 1 ML of C, and this independent of the electron energy. The calculations are performed in three steps. First, structural relaxation of the film system is performed until the forces become smaller than $0.001 \text{ eV}/\text{\AA}$ in order to determine the most stable geometry. Second, the electronic band structure is calculated using the LMTO method to determine the potential and charge distribution of the system's ground state. Finally, using the LKKR method and the converged potential the electron spin-motion angles of electrons reflected from Fe(001) and from 1 ML C/Fe(001) are obtained from the spin polarization \mathbf{P}' . We emphasize that the geometry of the spin-motion calculations is chosen identical to the experimental one.

Figure 30 shows the effect of carbon coverage on the calculated spin-motion angles ε and ϕ as a function of the electron primary energy. We can immediately conclude that 1 ML of carbon does not result in the breakdown of the

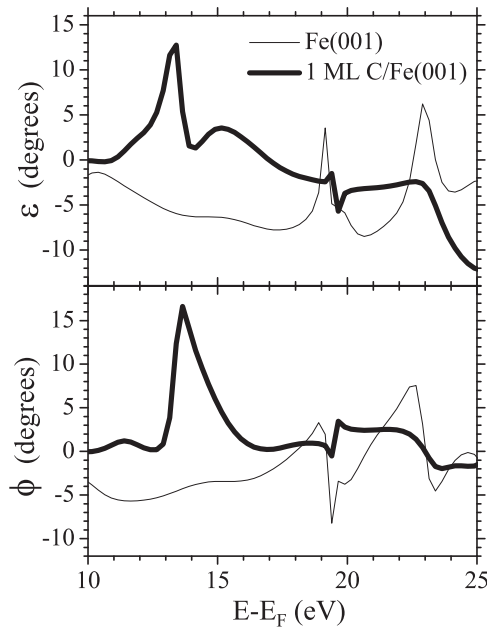


FIG. 30. Calculated ε (top) and ϕ (bottom) as a function of the electron energy for 9 ML of Fe(001) (thin line) and 1 ML of carbon on 9 ML of Fe(001) (thick line).

spin-motion angles. Instead it leads to more pronounced structures at certain energies compared to the Fe(001) case.

At this point we should emphasize that in the spin-motion calculations the electrons are scattered by a potential which is not supposed to be changed by the presence of the incident electrons. Thus, one might speculate that a possible modification of the scattering potential due to the incident electrons could be at the origin of the breakdown phenomenon. On the other hand, in this case the effect should depend on the incident electron intensity. However, we varied the incident current over several orders of magnitude but did not find any modification of the breakdown phenomenon. The only weakness of the SPLEED theory as it is implemented in the OMNI2K code is the fact that it is based on the muffin-tin approximation, where the potential is considered spherical in nonoverlapping muffin-tin spheres. This type of approximation, while it works nicely for metallic multilayers, might not describe well the scattering properties of a molecular or carbon layer on a metallic surface, where the charge transfer at the interface might play an important role [12].

M. Is the breakdown limited to exchange interaction?

There exist only two spin-dependent interactions of electrons with matter: exchange interaction and spin-orbit interaction. Up to now we have studied the effect of organic layer deposition on ferromagnetic substrates on physical quantities which are all governed only by exchange interaction. In fact, all quantities studied up to now were obtained in such a way that any effect resulting from spin-orbit interaction within the sample has been eliminated. Considering the fact that the breakdown phenomenon in the case of exchange interaction seems to be a very general phenomenon, we were wondering whether a similar effect would also appear in the case of spin-orbit interaction. For this we have performed in the first step experiments for which the initial spin polarization was oriented such that electron scattering both by exchange and by spin-orbit interaction could be studied. This allowed us to make a direct comparison between the breakdown phenomenon which is observed in experiments governed by exchange interaction and the behavior we observe in experiments governed by spin-orbit interaction. The initial spin polarization had both a component along the magnetization direction (for the measurement of the exchange asymmetry A_{ex}), which in our setup lies within the scattering plane (\mathbf{P}_0^{\parallel}), and a component perpendicular to the scattering plane (\mathbf{P}_0^{\perp}). The latter is necessary for measurement of the so-called spin-orbit asymmetry A_{so} , which is obtained by measuring the reflected electron intensity R in two spin configurations, namely, with \mathbf{P}_0^{\perp} parallel ($\uparrow\uparrow$) and antiparallel ($\uparrow\downarrow$) to the surface normal \mathbf{n} [71] of the scattering plane (normalized to the value of P_0^{\perp}):

$$A_{\text{so}} = \frac{1}{P_0^{\perp}} \frac{R(\mathbf{P}_0^{\perp} \uparrow\uparrow \mathbf{n}) - R(\mathbf{P}_0^{\perp} \uparrow\downarrow \mathbf{n})}{R(\mathbf{P}_0^{\perp} \uparrow\uparrow \mathbf{n}) + R(\mathbf{P}_0^{\perp} \uparrow\downarrow \mathbf{n})}.$$

As the first system we studied CoPc coverage on ferromagnetic Co(001). Figure 31 (top) shows both the exchange asymmetry A_{ex} and the spin-orbit asymmetry A_{so} as a function of the CoPc coverage. Both quantities exhibit the same strong change, leading to a very similar d_2 value of about 0.5 ML. The second system studied was CoPc/10 ML

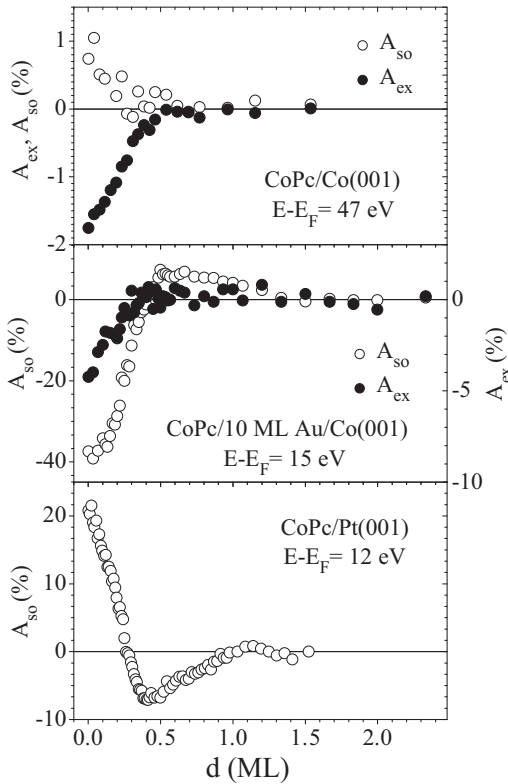


FIG. 31. Top: For the system CoPc/Co(001) A_{ex} and A_{so} are shown as a function of the CoPc thickness. The primary energy of the electrons is 47 eV. Middle: For the system CoPc/10 ML Au/Co(001) A_{ex} and A_{so} are shown as a function of the CoPc thickness. The primary energy of the electrons is 15 eV. Bottom: For the system CoPc/Pt(001) A_{so} is shown as a function of the CoPc thickness. The primary energy of the electrons is 12 eV.

Au/Co(001), in which the heavy element Au was supposed to lead to a much stronger spin-orbit asymmetry. Figure 31 (middle) again shows both A_{ex} and A_{so} as a function of the CoPc coverage. As in the preceding case both quantities exhibit the same behavior, with small differences. While A_{ex} becomes 0 for CoPc thicknesses larger than d_2 , A_{so} shows a sign change before reaching the saturation value d_2 and then decreases quite slowly (compared to the initial decline), to vanish, finally, for CoPc thicknesses above 1 ML. We note that this type of behavior was also observed in some “exchange” experiments. We thus conclude that the breakdown phenomenon is also present in “spin-orbit” experiments.

In the second step we performed experiments on the nonmagnetic substrate Pt(001). For these experiments we oriented the initial spin polarization perpendicular to the scattering plane. Figure 31 (bottom) shows A_{so} as a function of the CoPc coverage on Pt(001). Very similar behavior compared to the experiments with Au/Co as substrate is observed. This proves undoubtedly that the presence of a ferromagnetic system is not at all necessary to obtain the breakdown phenomenon.

We note that a combination of exchange and spin-orbit interaction can in general lead to an additional spin-dependent effect [72]. This effect can be envisioned as a situation in which exchange polarizes the incident electrons during the

scattering process, and they subsequently produce a spin-orbit-induced asymmetry (so-called Mott scattering). However, its presence can be neglected in the latter case, in which exchange interaction is absent.

V. CONCLUSION

By performing spin-polarized electron scattering experiments on different interfaces, consisting of different ferromagnetic and nonmagnetic metals as well as of different organic molecules and carbon, we observe completely unexpected behavior of the spin-polarized reflection properties of these interfaces. Submonolayer coverages of organic molecules or pure carbon make the electron reflection amplitude spin independent; i.e., both the reflectivity and the reflection phase become spin independent. The spin-motion angles are subject to a breakdown if a threshold value d_1 (between 0.1 and 0.25 ML, dependent on the system) is exceeded. We speculate that the latter corresponds to a percolation threshold. For thicknesses larger than d_2 (between 0.3 and 0.5 ML, dependent on the system) the spin-motion angles are 0 or, at least, very small compared to their initial values without coverage. We have shown that this behavior is a very general phenomenon and it is independent of

- (a) the energy of the primary electrons,
- (b) the choice of the metallic substrate,
- (c) the choice of the organic molecule, and
- (d) the orientation of the initial spin polarization.

It is not due to

- (a) a change in the surface magnetization,
- (b) depolarization of the primary electrons,
- (c) a “mirror” effect, or
- (d) direct interaction of the molecules with the ferromagnetic substrate.

Furthermore, the breakdown phenomenon is not limited to elastically scattered electrons and does not appear in transmission. Finally, it is shown that the breakdown phenomenon appears not only in exchange-governed experiments but also in experiments in which the spin-orbit interaction is the only spin-dependent interaction and where magnetism and thus the exchange interaction are absent.

Despite this wide range of results we are not able at the moment to identify the cause of this breakdown phenomenon. We suggest that the next step is to study this effect using an experimental method which combines spatial resolution at least in the nanometer range with sensitivity to the spin-dependent reflection amplitude: spin-polarized low-energy electron microscopy. Using spin-polarized electrons allows the measurement of both the exchange asymmetry A_{ex} and the spin-orbit asymmetry A_{so} , which have been shown to exhibit the breakdown phenomenon. Such spatially resolved experiments will allow us to study the spatial evolution of the breakdown phenomenon, in particular, in view of a possible percolation process, and might give us the additional information necessary to elucidate the processes which are behind this unexplained phenomenon.

ACKNOWLEDGMENTS

We acknowledge support from ANR Grant No. ANR-09-BLAN-0076-03. F. Djeghloul thanks Le Ministère

de l'enseignement Supérieur et de la Recherche Scientifique d'Algérie (MESRS) for financial support. We thank F. Le Normand (InESS, Strasbourg) for performing the Raman measurements on our carbon films. M. Gruber thanks W. Wulfhekel (KIT, Karlsruhe) for giving him the opportunity

to use his STM setup and the Franco-German university for support. Part of this work was performed using HPC resources from GENCI-CINES Grant No. 2013-gem1100 and those of the Meso Center of the University of Strasbourg.

-
- [1] V. A. Dediu, L. E. Hueso, I. Bergenti, and C. Taliani, *Nat. Mater.* **8**, 707 (2009).
- [2] N. Atodiressei, J. Brede, P. Lazic, V. Caciuc, G. Hoffmann, R. Wiesendanger, and S. Blügel, *Phys. Rev. Lett.* **105**, 066601 (2010).
- [3] C. Iacovita, M. V. Rastei, B. W. Heinrich, T. Brumme, J. Kortus, L. Limot, and J. P. Bucher, *Phys. Rev. Lett.* **101**, 116602 (2008).
- [4] H. Wende, M. Bernien, J. Luo, C. Sorg, N. Ponpandian, J. Kurde, J. Miguel, M. Piantek, X. Xu, Ph. Eckhold, W. Kuch, K. Baberschke, P. M. Panchmatia, B. Sanyal, P. M. Oppeneer, and O. Eriksson, *Nat. Mater.* **6**, 516 (2007).
- [5] M. Bowen, J.-L. Maurice, A. Barthélémy, M. Bibes, D. Imhoff, V. Bellini, R. Bertacco, D. Wortmann, P. Seneor, E. Jacquet, A. Vaurès, J. Humbert, J.-P. Contour, C. Colliex, S. Blügel, and P. H. Dederichs, *J. Phys. Condens. Mat.* **B 19**, 315208 (2007).
- [6] S. Sanvito, *Chem. Soc. Rev.* **40**, 3336 (2011).
- [7] T. Miyamachi, M. Gruber, V. Davesne, M. Bowen, S. Boukari, L. Joly, F. Scheurer, G. Rogez, T. K. Yamada, P. Ohresser, E. Beaurepaire, and W. Wulfhekel, *Nature Commun.* **3**, 938 (2012).
- [8] A. F. Takacs, F. Witt, S. Schmaus, T. Balashov, M. Bowen, E. Beaurepaire, and W. Wulfhekel, *Phys. Rev. B* **78**, 233404 (2008).
- [9] S. Javaid, M. Bowen, S. Boukari, L. Joly, J.-B. Beaufrand, X. Chen, Y. J. Dappe, F. Scheurer, J.-P. Kappler, J. Arabski, W. Wulfhekel, M. Alouani, and E. Beaurepaire, *Phys. Rev. Lett.* **105**, 077201 (2010).
- [10] S. Sanvito, *Nat. Phys.* **6**, 562 (2010).
- [11] C. Barraud, P. Seneor, R. Mattana, S. Fusil, K. Bouzehouane, C. Deranlot, P. Graziosi, L. Hueso, I. Bergenti, V. Dediu, F. Petroff, and A. Fert, *Nat. Phys.* **6**, 615 (2010).
- [12] F. Djeghloul, F. Ibrahim, M. Cantoni, M. Bowen, L. Joly, S. Boukari, P. Ohresser, F. Bertran, P. Le Fevre, P. Thakur, F. Scheurer, T. Miyamachi, R. Mattana, P. Seneor, A. Jaafar, C. Rinaldi, S. Javaid, J. Arabski, J.-P. Kappler, W. Wulfhekel, N. B. Brookes, R. Bertacco, A. Taleb-Ibrahimi, M. Alouani, E. Beaurepaire, and W. Weber, *Sci. Rep.* **3**, 1272 (2013).
- [13] D. T. Pierce, R. J. Celotta, G. C. Wang, W. N. Unertl, A. Galejs, C. E. Kuyatt, and S. R. Mielczarek, *Rev. Sci. Instrum.* **51**, 478 (1980), and references therein.
- [14] J. Kessler, *Polarized Electrons* (Springer, Berlin, 1985).
- [15] A. Clarke, G. Jennings, R. F. Willis, P. J. Rous, and J. B. Pendry, *Surf. Sci.* **187**, 327 (1987).
- [16] P. Krams, F. Lauks, R. L. Stamps, B. Hillebrands, and G. Güntherodt, *Phys. Rev. Lett.* **69**, 3674 (1992).
- [17] O. Hackmann, H. Magnan, P. le Fevre, D. Chandesris, and J. J. Rehr, *Surf. Sci.* **312**, 62 (1994).
- [18] U. Ramsperger, A. Vaterlaus, P. Pfäffli, U. Maier, and D. Pescia, *Phys. Rev. B* **53**, 8001 (1996).
- [19] G. C. Smith, H. A. Padmore, and C. Norris, *Surf. Sci.* **119**, L287 (1982).
- [20] B. Heinrich, S. T. Purcell, J. R. Dutcher, K. B. Urquhart, J. F. Cochran, and A. S. Arrott, *Phys. Rev. B* **38**, 12879 (1988).
- [21] P. J. Schurer, Z. Celinski, and B. Heinrich, *Phys. Rev. B* **51**, 2506 (1995).
- [22] H. Li, Y. S. Li, J. Quinn, D. Tian, J. Sokolov, F. Jona, and P. M. Marcus, *Phys. Rev. B* **42**, 9195 (1990).
- [23] S. De Rossi and F. Ciccacci, *Surf. Sci.* **307–309**, 496 (1994).
- [24] K. He, L. J. Zhang, X. C. Ma, J. F. Jia, Q. K. Xue, and Z. Q. Qiu, *Phys. Rev. B* **72**, 155432 (2005).
- [25] M. Stamparoni, A. Vaterlaus, M. Aeschlimann, and F. Meier, *Phys. Rev. Lett.* **59**, 2483 (1987).
- [26] L. Joly, L. T. Bismaths, F. Scheurer, and W. Weber, *Phys. Rev. B* **76**, 104415 (2007).
- [27] J. C. Buchholz and G. A. Somorjai, *J. Chem. Phys.* **66**, 573 (1977).
- [28] L. Joly, L. Tati-Bismaths, and W. Weber, *Phys. Rev. Lett.* **97**, 187404 (2006).
- [29] S. Tanuma, C. J. Powell, and D. R. Penn, *Surf. Interface Anal.* **21**, 165 (1994).
- [30] P. E. Laibinis, C. D. Bain, and G. M. Whitesides, *J. Phys. Chem.* **95**, 7017 (1991).
- [31] S. Modesti, S. Cerasari, and P. Rudolf, *Phys. Rev. Lett.* **71**, 2469 (1993).
- [32] M. R. C. Hunt, S. Modesti, P. Rudolf, and R. E. Palmer, *Phys. Rev. B* **51**, 10039 (1995).
- [33] A. Sellidji and B. E. Koel, *J. Phys. Chem* **97**, 10076 (1993).
- [34] C. Cepek, A. Goldoni, and S. Modesti, *Phys. Rev. B* **53**, 7466 (1996).
- [35] S. Tanuma, T. Shiratori, T. Kimura, K. Goto, S. Ichimura, and C. J. Powell, *Surf. Interface Anal.* **37**, 833 (2005).
- [36] P. K. Chu and L. Li, *Mater. Chem. Phys.* **96**, 253 (2006).
- [37] F. Petraki and S. Kennou, *Int. J. Nanotechnol.* **6**, 112 (2009).
- [38] F. Petraki, V. Papaefthimiou, and S. Kennou, *Organ. Electron.* **8**, 522 (2007).
- [39] B. J. Topham, M. Kumar, and Z. G. Soos, *Adv. Funct. Mater.* **21**, 1931 (2011).
- [40] S. Javaid, S. Lebégue, B. Detlefs, F. Ibrahim, F. Djeghloul, M. Bowen, S. Boukari, T. Miyamachi, J. Arabski, D. Spor, J. Zegenhagen, W. Wulfhekel, W. Weber, E. Beaurepaire, and M. Alouani, *Phys. Rev. B* **87**, 155418 (2013).
- [41] F. Wilhelm, M. Angelakeris, N. Jaouen, P. Pouloupoulos, E. T. Papaioannou, C. Mueller, P. Fumagalli, A. Rogalev, and N. K. Flevaris, *Phys. Rev. B* **69**, 220404(R) (2004).
- [42] T. L. Francis, O. Mermer, G. Veeraraghavan, and M. Wohlgenannt, *New J. Phys.* **6**, 185 (2004).
- [43] T. D. Nguyen, Y. Sheng, J. Rybicki, G. Veeraraghavan, and M. Wohlgenannt, *J. Mater. Chem.* **17**, 1995 (2007).
- [44] Z. H. Cheng, L. Gao, Z. T. Deng, N. Jiang, Q. Liu, D. X. Shi, S. X. Du, H. M. Guo, and H.-J. Gao, *J. Phys. Chem. C* **111**, 9240 (2007).
- [45] S. M. Barlow and R. Raval, *Surf. Sci. Rep.* **50**, 201 (2003).

- [46] Y. Hosoi, Y. Sakurai, M. Yamamoto, H. Ishii, Y. Ouchi, and K. Seki, *Surf. Sci.* **515**, 157 (2002).
- [47] O. Marchenko and J. Cousty, *Phys. Rev. Lett.* **84**, 5363 (2000).
- [48] M. Lackinger, S. Griessl, W. M. Heckl, and M. Hietschold, *J. Phys. Chem. B* **106**, 4482 (2002).
- [49] M. Abel, A. Dimitriev, R. Fasel, N. Lin, J. V. Barth, and K. Kern, *Phys. Rev. B* **67**, 245407 (2003).
- [50] J. A. Gardener, G. A. D. Briggs, and M. R. Castell, *Phys. Rev. B* **80**, 235434 (2009).
- [51] W. Weber, D. Kerkmann, D. Pescia, D. A. Wesner, and G. Güntherodt, *Phys. Rev. Lett.* **65**, 2058 (1990).
- [52] T. G. Walker and H. Hopster, *Phys. Rev. B* **48**, 3563 (1993).
- [53] T. G. Walker, A. W. Pang, H. Hopster, and S. F. Alvarado, *Phys. Rev. Lett.* **69**, 1121 (1992).
- [54] T. G. Walker and H. Hopster, *Phys. Rev. B* **49**, 7687 (1994).
- [55] W. Weber (unpublished).
- [56] A. Scholl, L. Baumgarten, and W. Eberhardt, *Phys. Rev. B* **56**, 747 (1997).
- [57] D. Oberli, R. Burgermeister, S. Riesen, W. Weber, and H. C. Siegmann, *Phys. Rev. Lett.* **81**, 4228 (1998).
- [58] M. S. Hammond, G. Fahsold, and J. Kirschner, *Phys. Rev. B* **45**, 6131 (1992).
- [59] M. Aeschlimann, M. Bauer, S. Pawlik, W. Weber, R. Burgermeister, D. Oberli, and H. C. Siegmann, *Phys. Rev. Lett.* **79**, 5158 (1997).
- [60] O. K. Andersen, *Phys. Rev. Lett.* **8**, 149 (1964).
- [61] <http://www.fkf.mpg.de/andersen/LMTODOC/LMTODOC.html>.
- [62] J. Koringa, *Physica* **13**, 392 (1947).
- [63] W. Kohn and N. Rostoker, *Phys. Rev.* **94**, 1111 (1954).
- [64] P. Weinberger, *Electron Scattering Theory of Ordered and Disordered Matter* (Clarendon, Oxford, UK, 1990).
- [65] A. Gonis, *Green Functions for Ordered and Disordered Systems. Studies in Mathematical Physics* (North-Holland, Amsterdam, 1992), Vol. 4.
- [66] R. Feder, *J. Phys. C: Solid State Phys.* **14**, 2049 (1981).
- [67] Edited by R. Feder, in *Advanced Series in Surface Science* (World Scientific, Singapore, 1985), Chap. 4.
- [68] J. Henk, in *Handbook of Thin Film Materials, Vol. 2. Characterization and Spectroscopy*, edited by H. S. Nalwa (Academic Press, New York, 2001), Chap. 10.
- [69] T. Berdot, A. Hallal, L. T. Bismaths, L. Joly, P. Dey, J. Henk, M. Alouani, and W. Weber, *Phys. Rev. B* **82**, 172407 (2010).
- [70] A. Hallal, T. Berdot, P. Dey, L. T. Bismaths, L. Joly, A. Bourzami, F. Scheurer, H. Bulou, J. Henk, M. Alouani, and W. Weber, *Phys. Rev. Lett.* **107**, 087203 (2011).
- [71] The surface normal \mathbf{n} of the scattering plane is given by $\mathbf{n} = (\mathbf{k}_i \times \mathbf{k}_s) / |\mathbf{k}_i \times \mathbf{k}_s|$, where \mathbf{k}_i and \mathbf{k}_s are the wave vectors of the incident and the scattered electrons, respectively.
- [72] P. G. Burke and J. F. B. Mitchell, *J. Phys. B* **7**, 214 (1974).